Mineral mapping and in-situ Rb-Sr dating of Proterozoic Glauconites

Hamed Mohammed Alsarakhi November 2018
Word count- 4257

THE UNIVERSITY
of ADELAIDE

TITLE:

MINERAL MAPPING AND IN-SITU Rb-SR DATING OF PROTEROZOIC GLAUCONITES

RUNNING TITLE:

MINERAL MAPPING AND DATING OF GLAUCONITE

ABSTRACT:

Precise and accurate dating of glauconites in marine sediments and sedimentary rocks is of high interest to both basin exploration purposes as well as earth system evolution studies.

This project tests the new in-situ Rb/Sr dating method of glauconites using LA-ICP MS/MS system, and analyses samples of glauconites from selected Indian Basins, including the Vindhyan Basin, Chhattisgarh Basin and Kutch Basin. Previous studies report the ages of glauconite samples collected from these basins using different and more established methods such as K-Ar and TIMS-based Rb-Sr dating. These popular methods have however the problem of possible contamination of bulk glauconite sample (typically consisting of tens to hundreds of separated glauconite grains) with older detrital minerals and/or younger clay minerals. The new in-situ Rb/Sr dating method used in this project in combination with detail mineral mapping of samples (Nanomin technique) have potential to overcome the above problems and analytical issues. As to results, the samples analysed by in-situ Rb/Sr method including samples: G2 (Vindhyan Basin Semri Group) , G6 (Vindhyan Basin Semri Group Chitrakoot Fm), G8 (Chhattisgarh Basin Raipur Group) and G10 (Kutch Basin) yielded, respectively, the

following Rb/Sr ages of 1454 ±14 Ma, 1386 ±25 Ma, 920 ±12 Ma and 127 ±36 Ma.

These in-situ Rb/Sr ages for most part agree with the published ages for equivalent

glauconite samples from these basins analysed by K/Ar and/or TIMS-based Rb/Sr

techniques.

KEYWORDS:

MINERAL MAPPING, RB-SR, DATING, PROTEROZOIC, GLAUCONITE, INDIAN BASINS, IOLITE, NANOMIN.

TABLE OF CONTENTS

LIST OF FIGURES AND TABLES:

INTRODUCTION:

Glauconite is phyllosilicate clay mineral forming typically a sand sized green mineral grains with the following general chemical formula: $(K,Na) (Fe^{3+}, Al, Mg)_2 (Si, Al)_4 O_{10} (OH)_2$. Marine glauconite requires specific redox and chemical conditions to form which normally form below sea level at depths between 30 to 1,000 meters, near-normal salinity, reducing conditions (oxygen poor zones), and appropriate source materials and cations/anions for mineral formation. In general, there are three processes that lead to formation of marine glauconite which are: (i) Fecal pellets alteration of the bottom-dwelling creatures, (ii) Particles alterations of the illitic and biotitic clays by the seawater, and (iii) the straight precipitation from seawater and/or sediment pore fluids (Banerjee et al. 2016). Glauconite formation is also favoured by high organic content of the bottom sediments in which it forms, and by slow and/or minimum sedimentation rates under a fairly wide range of temperatures. Chemical conditions of glauconite suggests that it forms as a result of partial reduction of Iron (Fe^{+3} to Fe^{+2}), but pH of local seawater or pore fluids seems to be not of great importance to the glauconite formation as it can form in sandstones (low pH, acidic) to carbonate-dominated (high pH or basic) systems, thus covering a wide range of pH conditions.

The mineralogical content of typical marine glauconite assemblages ranges from glauconite-smectite to glauconite-mica end-members. Also, these glauconite groups differ in structure and composition, and younger glauconite (Phanerozoic) contains low potassium and iron portions but higher aluminium, whereas older (Precambrian) glauconites have typically higher potassium and iron and lower aluminium contents (Banerjee et al. 2016). However, younger glauconites are also mineralogically more heterogeneous than older glauconites (Hower 1961; Hegab et al 2016). Thus, the

4

mineralogical content and chemical composition are indicative of the maturity of the

glauconite assemblages.

Classification of glauconite formation, during the evolution of the grains, can be divided

into four main stages based on the mineralogical/chemical composition, including: (i)

nascent, (ii) slightly evolved, (iii) evolved, and (iv) highly evolved or mature

glauconites, as shown in Figure 1 (Hegab et al. 2016).
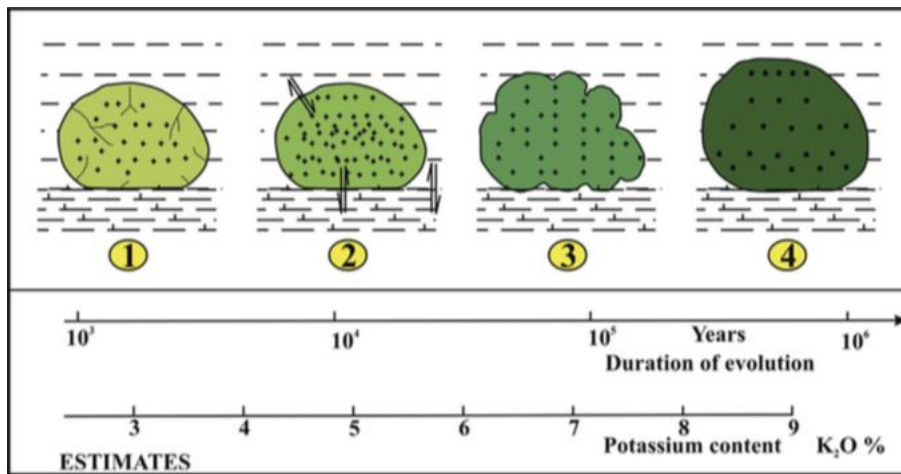
Figure 1: The evolution of glauconite showing the four stages of evolution including: 1. Nascent, 2. Slightly evolved, 3. Evolved, 4. Highly evolved or mature (from Hehab et al. 2016).

In terms of applications to geology and earth sciences, glauconite is an important

mineral whose dating can determine the age of the sediment formation as the mineral

forms early on during the initial or early stage of sediment diagenesis, typically right

after sediment deposition (e.g., within first thousands to hundreds of thousand years:

~10^3 to ~10^5 years, Hehab et al. 2016). In this study, we will determine the age of

glauconite samples from different Proterozoic Indian basins using a novel laser ablation

(LA) based Rb/Sr dating method via LA-ICP MS/MS (Zack et al. 2017), complemented

by detail mineral mapping of analysed samples (Nanomin Images, Rahman et al., 2018).

Previous studies have successfully dated glauconites using different methods such as

TIMS-based Rb-Sr and K-Ar dating (Kumar et al., 2001, Baldermann et al. 2017,

Banerjee et al. 2016). These established methods, however, have the problem of possible contamination of "bulk" analysed glauconite samples (typically consisting of a few hundred separated mineral grains) that need to be processed and/or dissolved as single "bulk" sample for dating. Such composite "glauconite samples" however commonly also contain tracers of older detrital minerals (e.g. feldspars) or younger Fe-smectites (e.g. nontronites), which can thus bias the Rb/Sr and K/Ca age acquired from these "bulk" samples, limiting the precision and accuracy of these traditional dating methods. In addition, K/Ar and/or K/Ca isotope systems have fairly low closure temperatures, estimated around 80-90 C, and thus these dating techniques are quite sensitive to thermal resetting due to higher burial diagenesis and/or later alteration events (Derkowski et al. 2009; Baldermann et al. 2017). Therefore, the new micro-scale LA-based method for Rb/Sr dating can be used to minimise some of these problems (e.g., avoiding dating of admixed detrital mineral phases, or altered glauconite zones), and this project explores the suitability of such approach for dating of Proterozoic and Phanerozoic glauconites from selected Indian Basins (Vindhyan, Chhattisgarh and Kutch Basins). In addition, the project also aims to investigate if single-grain Rb/Sr dating is feasible with such novel LA-based ICP MS/MS technique, by collecting data from multiple LA spots across larger and well-preserved glauconite grains. This study is also going to test the homogeneity of Rb and Sr isotope compositions across selected larger glauconite grains, with implications for possible intra-grain difference in acquired Rb/Sr ages in a single grain due to element diffusion and/or selective grain alteration (e.g. a rim is more altered than the grain's inner core?). Finally, the acquired LA-based Rb/Sr ages of studied Proterozoic and Phanerozoic glauconites are then compared to published ages for these glauconite samples (or rather equivalent samples collected

from the same stratigraphic units) determined by alternative dating method such as TIMS-based Rb/Sr (Kumar et al., 2001) and/or K/Ar geochronology (Banal et al., 2017, Rathore et al. 1999).

GEOLOGICAL BACKGROUND - INDIAN BASINS AND GLAUCONITE SAMPLES

THE VINDHYAN BASIN, SEMRI GROUP – PROTEROZOIC GLAUCONITES (SAMPLES G2 and G6)

The Vindhyan Basin is the largest Proterozoic depositional system in India, located in the central part of the Indian subcontinent, and is surrounded by other Proterozoic basins and sub-basins including Chattisgarh, Cuddapah and Bikaner-Ngaur Basins (see Figures 2 and 3). The Vindhyan Basin is a characteristic intracontinental Proterozoic basin which is exposed in three main Indian regions: Bundelkhand, Son valley and Rajasthan, and these exposures contain Proterozoic sedimentary sequences of shales, sandstones and limestones (Ram 2012).

The Vindhyan Basin covers an area of about 80,000 km^2 and extends into the Ganga valle,y underneath the foredeep tertiary Himalayan sediments in the northern and north-eastern parts, and in the southwestern parts the younger Deccan volcanic cover the basin. The Vindhyan Basin is also a prospective petroleum system containing the organic rich source rocks (shales), and suitable carbonate and sandstone reservoirs and hydrocarbon traps (Ram, 2012).

Figure 2: The locations of Proterozoic basins in India (from Ram, 2012).
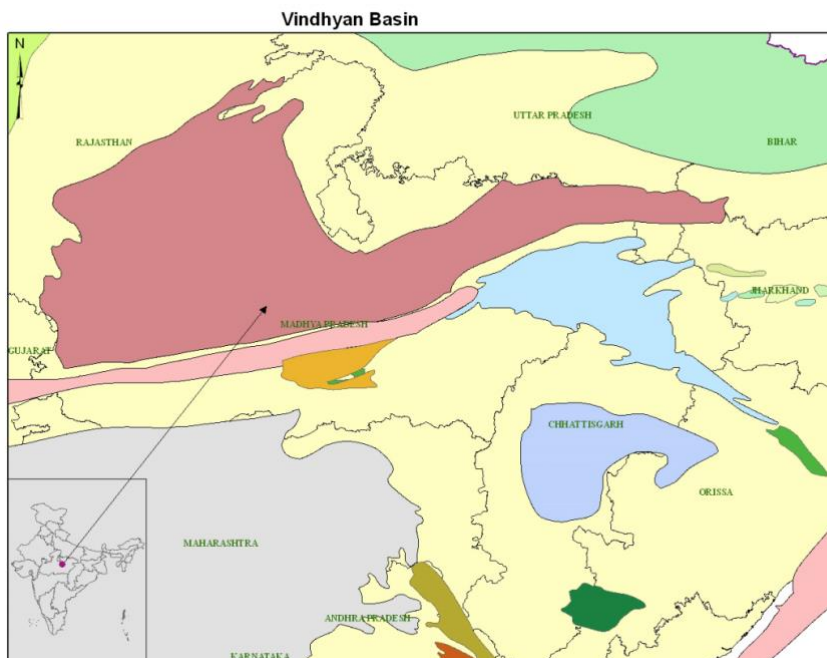
Figure 3: A detail map of the Proterozoic Vindhyan Basin (pointed by the arrow) in the central part of the India, showing also the main states and provinces to which the basin extents in the central Indian region (from Dirctorate General Of Hydrocarbon 2017).

Based on published Rb-Sr dating of Glauconites in the northern part of the Vindhyan

Basin, in the Chitrakut area, the expected formation age of these Proterozoic glauconite

samples ranges from ~1409 to ~1531 Ma, as shown in the table below (data from

Kumar et al 2001).

Sample	Rb (ppm)	Sr (ppm)	$^{87}Rb/^{86}Sr$ (atomic)	$^{87}Sr/^{86}Sr$ (atomic)	Model age (Ma)
S.9	348	5.27	308	6.92400 ± 8	1409 ± 14
S.3	315	5.00	295	6.98466 ± 3	1483 ± 15
LN.1	308	4.77	309	7.37651 ± 15	1504 ± 15
LN.4	322	5.22	281	6.59281 ± 12	1461 ± 14
LS.4	266	14.80	58.4	1.99030 ± 4	1531 ± 15
LS.9	304	13.30	76.6	2.29901 ± 15	1449 ± 14

Table 1: The Rb-Sr data of Vindhyan basin glauconites for different samles using an initial ratio of 0.7066 (from Kumar et al 2001).

		————— Unconfomity —————	
Upper Vindhyan	Bhander Group	Sand, shale and limestone	
	Rewa Group	Sandstone and shale	
	Kaimur Group	Sandstone and shale	
		— Unconformity —	
Lower Vindhyan	Semri Group	Rohtas Subgroup	Bhagwar shale Rohtas limestone
		Kheinjua Subgroup	Rampur shale Chorhat sandstone Koldaha shale
		Mirzapur Subgroup	Deonar porcellanite Kajrahat limestone Basal shale Deoland quartzite
		— Unconformity —	
	Metamorphics and granites		

Table 2: The stratigraphic succession of Vindhyan supergroup extending in the Son Valley (from Kumar et al 2001).

CHHATTISGARH BASIN, RAIPUR GROUP – PROTEROZOIC GLAUCONITES (SAMPLE G8)

Chhattisgarh Basin is considered to be the third largest and one of the best geo-chronologically constrained Proterozoic Indian basins covering an area of about 33,000 km^2 and containing a 2,300 m thick mixed carbonate and phosphorite/evaporite sequence (Ram, 2012). Chhattisgarh Basin is located in the middle to the eastern part of India at the northern edge of Bastar Craton extending for about 300 km in the E-W and 200 km in the N-S directions. The geological maps of the Chhattisgarh basin show a meta-sedimentary and metavolcanics rocks of unclassified Archean gneisses of TTG – Tonalite, Trondhjemite, Granodiorite- in the southern part of the basin. Chhattisgarh Basin supergroup is divided into three main unconformity groups including: Singhora, Chandsupur and Raipur. Several studies used different dating methods such as zircon tried to construct the time domain of the Chhattisgarh Basin sediments. Summarizing the recently reported geo-chronological studies (Ram, 2012, Chakraborty et al 2015), the Chhattisgarh Basin belongs to Mesoproterozoic with a history of sedimentation spanning for about 400 Ma, from ~1405 ± 9Ma up to about ~1000 Ma, the latter constrained by Rb-Sr dating of Raipur group at 993 ± 8Ma (Chakraborty et al 2015). Table 3 shows the geochronological data from different times using different methods.

A REVIEW OF CHHATTISGARH GEOLOGY
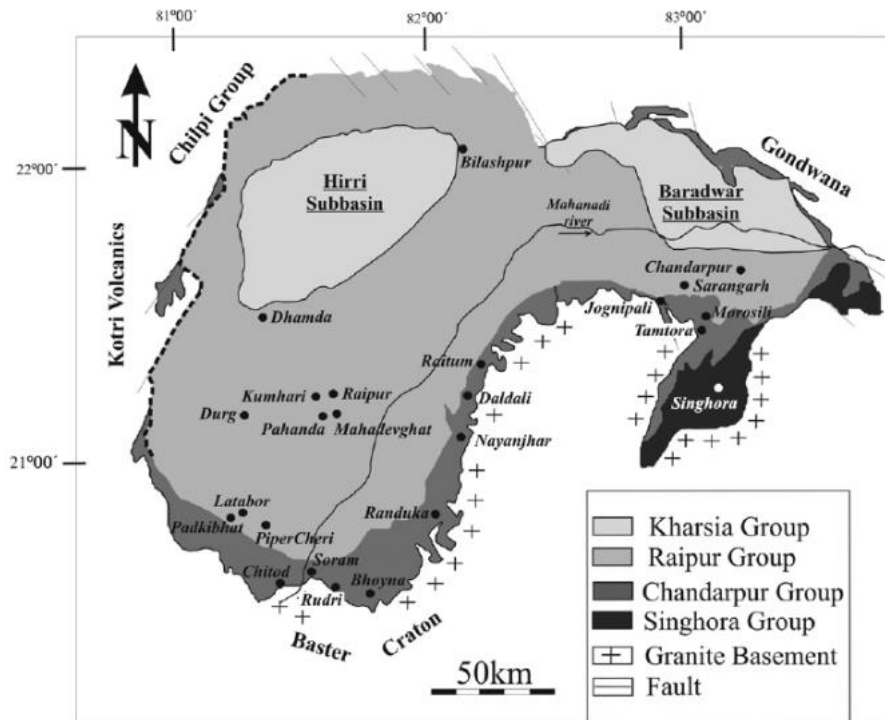
Figure 4: The location of Chhattisgarh Basin showing the extent of the basin at the edge of Bastar Craton in India, see also Figure 2 (from Chakraborty et al 2015).

	Dated rock	Methods	Kharsiya Group	Raipur Group	Chandarpur Group	Singhora Group
Pandey *et al.* (2012)	Dolerite Intrusive	Rb–Sr, internal isochron			1641 ± 120 Ma	
Bickford *et al.* (2011a–c)	Porcellanite	U–Pb SHRIMP		993 ± 8 Ma		1405 ± 9 Ma
Sinha *et al.* (2011)	Dolerite Sill	Rb–Sr, whole-rock isochron				1121 ± 742 Ma
Das *et al.* (2011)	Diabasic intrusive					1421 ± 23 Ma
Das *et al.* (2009)	Porcellanite					*c.* 1500 Ma
Patranabis-Deb *et al.* (2007)	Porcellanite			910 ± 1021 Ma		

Table 3: Geochronological data from different times using different methods (Chakraborty et al 2015).

THE KUTCH BASIN – CRETACEOUS GLAUCONITES (SAMPLE G10)

The Kutch Basin is a peri-continental embayed basin lodging a rift graben (Rathore, 1999). It is located in the north-western part of India extending in the north from the Great Rann of Kutch to the Kathiawar Peninsula in the south. The Kutch sedimentary rift basin is distinctively characterised by end of lower Cretaceous transgressive/ regressive well-defined sequences. The basin spreads offshore forming a wide shelf platform filled with more than 3 km thick Mesozoic sediments overlie by 900m thin Tertiary sequence (Rathore et al. 1999; National Data Repository 2015).

Sl. No.	Sample No.	Sample Location	K (wt %)	Total ^{40}Ar (x 10^{-7} cc STP g^{-1})	Rad ^{40}Ar	Age (± 2σ) Ma
1	Ukra$_{KT}$-1N	Katesar Temple	5.42	304.56	234.08	107.9±3.4
2	Ukra$_{KT}$-1A	Katesar Temple	5.42	291.42	226.36	104.4±3.2
3	Ukra$_{KT}$-1AD	Katesar Temple	5.42	301.84	224.39	103.6±3.2
4	Ukra$_{KT}$-4N	Katesar Temple	5.64	281.16	238.11	105.5±3.3
5	Ukra$_{KT}$-4B	Katesar Temple	5.64	284.93	240.43	106.5±3.3
6	Ukra$_{UH}$-3N	Ukra Hill	5.91	259.63	244.51	103.5±3.4
7	GL-O$^{\$}$	-	6.46	298.408	243.086	94.3±2.8

Table 4: The K/Ca age data of different glauconite samples from selected locations in the Kutch Basin. note that, N is Untreated sample, A is sample treated 0.5N HCl, B is sample treated with 0.1N HCl, D is duplicate analysis and GL-O is glauconite standard wit age of 95.03±1.11 Ma (Rathore et al. 1999, see also Derkowski et al. 2009).

METHODS

SAMPLE PREPARATION – POLISHED GLAUCONITE MOUNTS

Prior to analysis, all glauconite samples (i.e. glauconite grains in rock chips) were cut and embedded into a resin. After that, the samples were polished mechanically with SiC paper and then multiple times with microdiamond paste (from coarser down to final 2 microns paste) to remove any surface irregularities and to polish the glauconite grains. Samples were sent to Adelaide Microscopy to get carbon-coated before imaging and detail mineral mapping (see below).

MINERL MAPPING OF GLAUCONITE SAMPLE – NANOMIN TECHNIQUE

Detail micro-scale mineral mapping of studied samples was done using the FEI Teneo emission Scanning Electron Microscope (SEM) equipped with dual Energy Dispersive X-ray Spectroscopy (EDS) detectors (Bruker X Flash Series 6) in Sydney at Macquarie University. The SEM analysis was performed at 13 mm working distance and 15kV accelerating voltage. Mineral mapping EDS spectra was collected simultaneously at 200 nm steps and 8 ms acquisition times using the FEI Maps Mineralogy software. Individual EDS spectra were then classified using the FEI Nanomin software, which was achieved by comparing EDS spectra in the mapped area against known reference spectra of mineral standards (for details see Falster et al. 2018; Rahman et al. 2018).

IN-SITU RB/SR DATING OF GLAUCONITES VIA LA-ICP MS/MS

A single collector ICP MS/MS instrument (Agilent 8900) equipped with a collision cell and coupled to a Laser Ablation (LA) system (ASI RESOlution 193 Eximer laser) was used for in-situ Rb/Sr dating of glauconite samples. Table 5 shows the instrument's settings and laser parameters used on LA-ICP MS/MS Rb/Sr dating. To separate Rb from Sr, N_2O gas has been used as a reaction gas due to the high tendency of Sr to react with oxygen (see below) which is not the case for Rb (Zack et al. 2016).

$$^{87}Sr + {}^{16}O \implies {}^{103}SrO$$

$$^{86}Sr + {}^{16}O \implies {}^{102}SrO$$
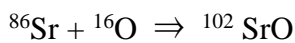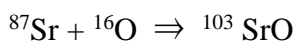
The LA-ICP MS/MS system used consists of two main quadrupoles (Q1 and Q2) placed on both sides of the gas reaction or collision cell (see Figure XY). By using the MS/MS mode, all the matrix ions that have a different m/z ratio from the respective analyte ions (isotopic ions) will be removed by the first quadrupole (Q1). Then, the isotopic ions will react with the reaction gas (N_2O) and thus, their masses will be shifted (i.e., a mass shifted mode for data collections: ^{87}Sr collected at mass 103 as $^{87}Sr^{16}O$ species). The mass shifted ions of interest, ^{86}Sr and ^{87}Sr, will be then collected by the detector after being filtered throg the second quadrupole (Q2) as measured as masses 102 and 103, respectively,
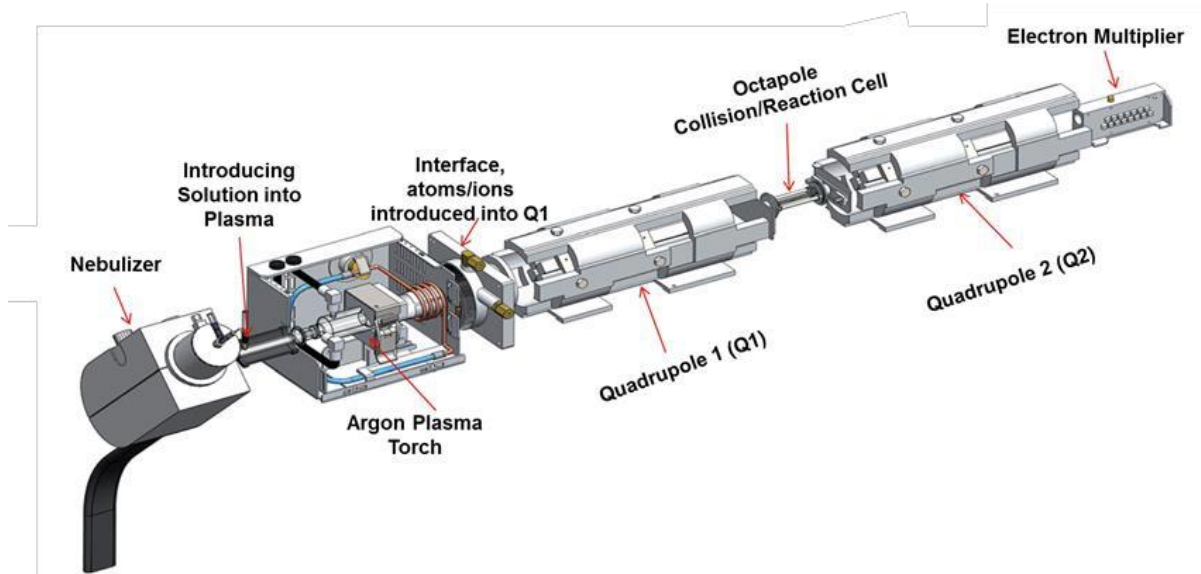
Figure 5: The set-up of the quadrupoles (Q1 &Q2) and a collision cell within the Agilent 8900 ICP MS/MS instrument (from Jensen 2017).

All the settings and running parameters that have been used for LA-ICP MS/MS are shown in the table below:

Scan type: **MS/MS**
- Fluence $3.5 J/cm^3$
- Pulse rate   5 Hz
- Spot size   74 μ

Tune parameters:
- Plasma Mode   --
- Nebulizer Gas (Ar) 1 L/min
- RF Power   1350 w
- Auxiliary Gas 0.90 L/min
- RF Matching   1.18 V
- Plasma Gas 15 L/min
- Sample Depth   4 mm

Lens Parameters:
- Extract 1   -2 V
- Q1 Entrance 2 V
- Cell Exit   -150 V
- Extract 2   -150 V
- Q1 Exit   -1 V
- Deflect   -10 V
- Omega Bias   -75 V
- Cell Focus   -2 V
- Plate Bias -80 V
- Omega Lens   7 V
- Cell Entrance -100 V

Q1 Parameters:
- Q1 Bias   -2 V
- Q1 Prefilter Bias -9 V
- Q1 Postfilter Bias -10 V

Cell Parameters:
- Use Gas   Yes
- 3rd Gas Flow   0%
- Axial Acceleration 2 V
- He Flow   0 mL/min
- 4th Gas Flow (N_2O) 35%
- OctP RF   180 V
- H_2 Flow   0 mL/min
- OctP Bias   -23 V
- Energy Discrimination -10 V

Q2 Parameters:
- Q2 Bias   -33 V

Table 5: The settings and Parameters used for LA-ICP MS/MS system.

DATA PROCESSING - IOLITE AND ISOPLOT

The reduction of the raw data obtained by the LA-ICP MS/MS and shown in the Appendix, was important and critical step for reliable in-situ Rb/Sr dating. All data were first normalised to nanopowder standard MicaMg (see Zack et al. 2016), using Iolite Software and then plotted in Isoplot Software to calculate the corresponding Rb/Sr ages (see below). The reduction process in Iolite includes the subtraction of baseline, correction of raw data with respect to selected standard (MicaMg), and calculation of corrected $^{87}Rb/^{86}Sr$ and $^{87}Sr/^{86}Sr$ ratios (Zack et al. 2016). The reduced and corrected data were then exported as "data columns" in Excel format and then manipulated in Isoplot Software to calculate the corresponding Rb/Sr age via isochrones. For the latter, this study uses a new ^{87}Rb decay constant from Villa et al (2015) of 1.3972 ± 0.0045 x 10^{-11} years. Isochrons were produced assuming an initial $^{87}Sr/^{86}Sr$ ratio of the expected Sr isotope composition of coeval paleo-seawater (Shields and Veizer, 2002), based on the published ages of the studied glauconite samples from Vindhyan, Chhattisgarh and Kutch Basins (i.e., Mid-Proterozoic, Neoproterozoic and Cretaceous ages, respectively). For details see also Figure 6 below.
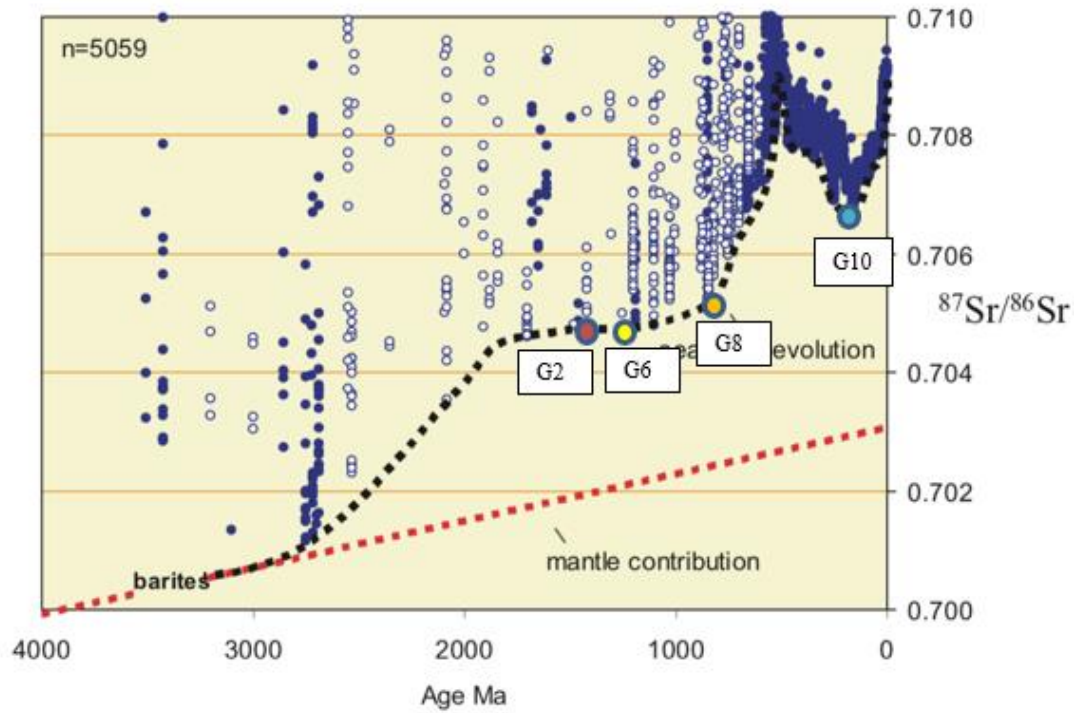
Figure 6: Strontium isotopic ($^{87}Sr/^{86}Sr$) evolution of seawater based on analysed Precambrian carbonate rocks and Phanerozoic fossils (from Shields and Veizer, 2002).. The labels in white boxes are representing expected ages of different glauconite samples, and the colour circles are the corresponding $^{87}Sr/^{86}Sr$ signatures of coeval paleo-seawater during these times, which were used as "initials" for age calculations in Isoplot Software.

RESULTS AND OBSERVATIONS

Glauconite Sample G2 - Vindhyan Basin, Semri Group
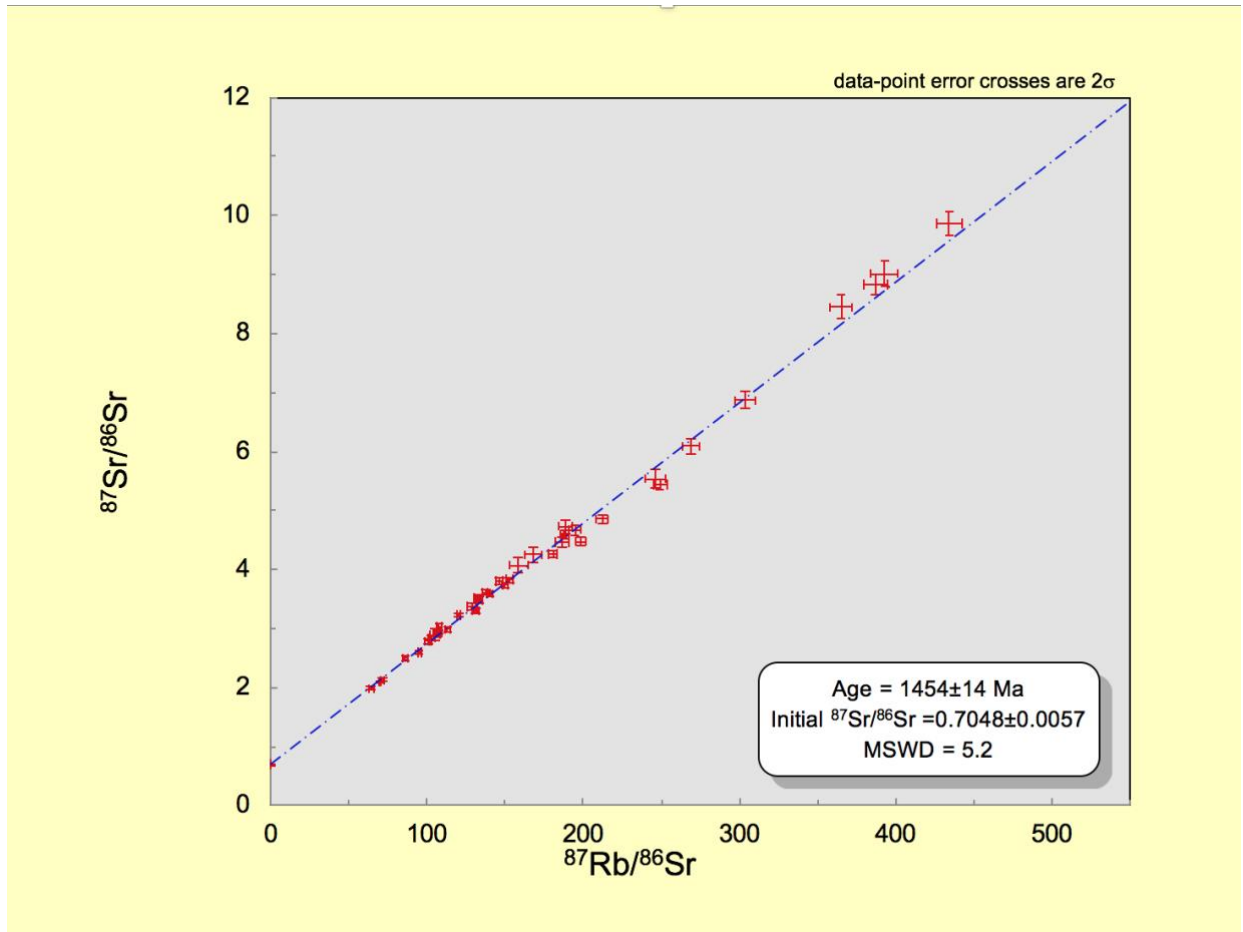
Figure 7: In-situ Rb/Sr age from a sample of mid-Proterozoic glauconites (G2) from Vindhyan Basin. Isochron showing an age of about 1454± 14 Ma using an initial ^{87}Sr/^{86} Sr of 0.705 for mid-Proterozoic seawater Sr isotope composition (see Shields and Veizer, 2002) .

The constructed isochron (Figure 10) for the sample G2 from Vindhyan Basin (Semari

Group) yielded a Rb/Sr age of 1454 ± 14 Ma (MSWD value of 5.2) using an initial

^{87}Sr/^{86} Sr of 0.705. The MSWD stands for Mean Standard Weight Deviation in isotopic

dating which is a measure of how close the points are to the constructed regression line

or isochrone (i.e., goodness of fit, or the smaller the MSWD the closer the data plot to

an isochrone). A MSWD value less or equal to 1 means a good fit (i.e., data overlap

with the isochrone within their analytical errors). On the other hand, a value greater than

1 indicates that there is a "natural scatter" outside of the analytical errors that is likely related to geological factor (White 2013), e.g, some samples are older or younger than the mean age defined by the isochrones, or the Rb/Sr system in selected samples have been partially reset. Overall, the acquired data from G2 sample show a fairly good but not perfect MSWD of ~5, and most of the data plot along or close to the constructed isochrone. However, the larger MSWD suggest that there might be more than one glauconite population, and some grains might originate from redeposited older populations.
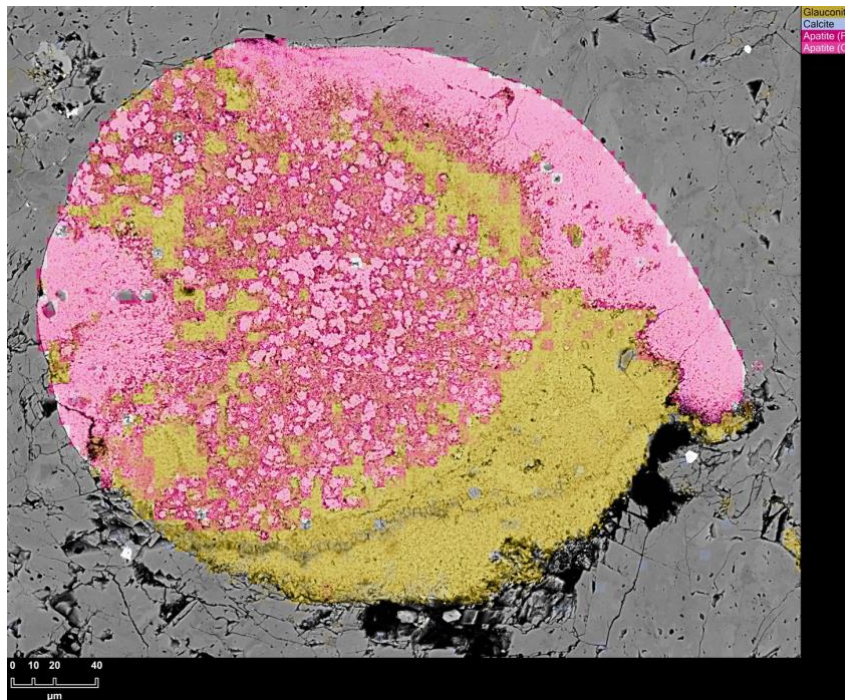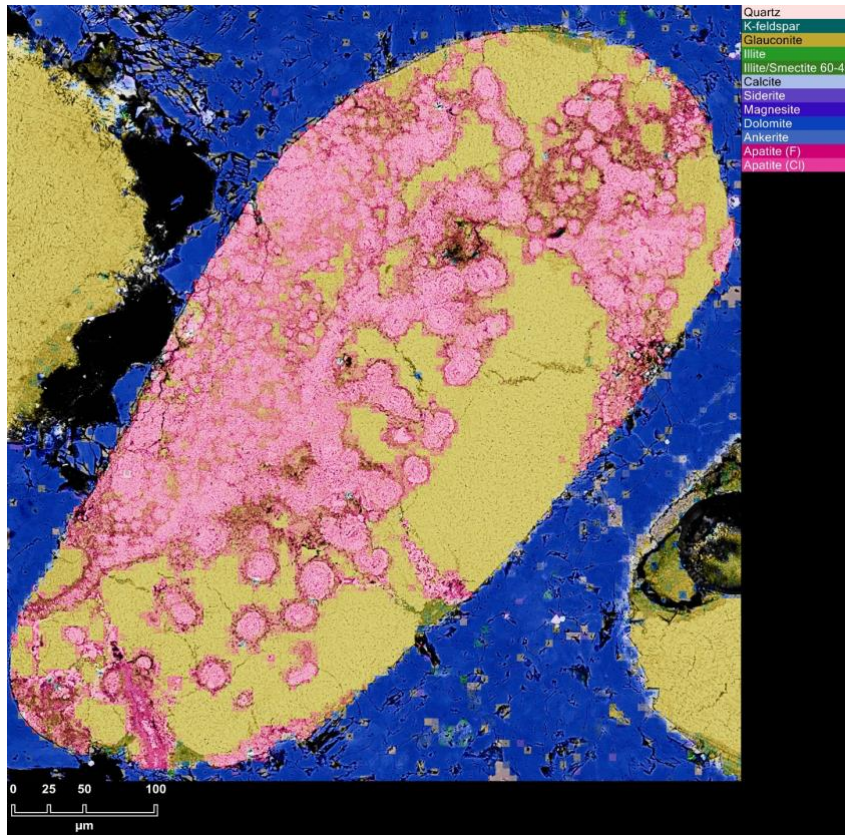
Figure 8: Mineral map of selected altered glauconite grains (brown) from sample G2, which were not analysed for Rb/Sr dating due to their alteration and replacement by apatite (pink). Surrounding matrix is composed of dolomite (blue) and calcite (grey) for sampl

Figure 6, top panel shows glauconite grains (brown) with apatite (pink) in a matrix of

dolomite (blue). Where the bottom image shows a glauconite grain with apatite as well

as calcite (grey) surrounding the grain. Also, no laser spots observed on the image as

these altered glauconite grains were not targeted for in-situ Rb/Sr dating.
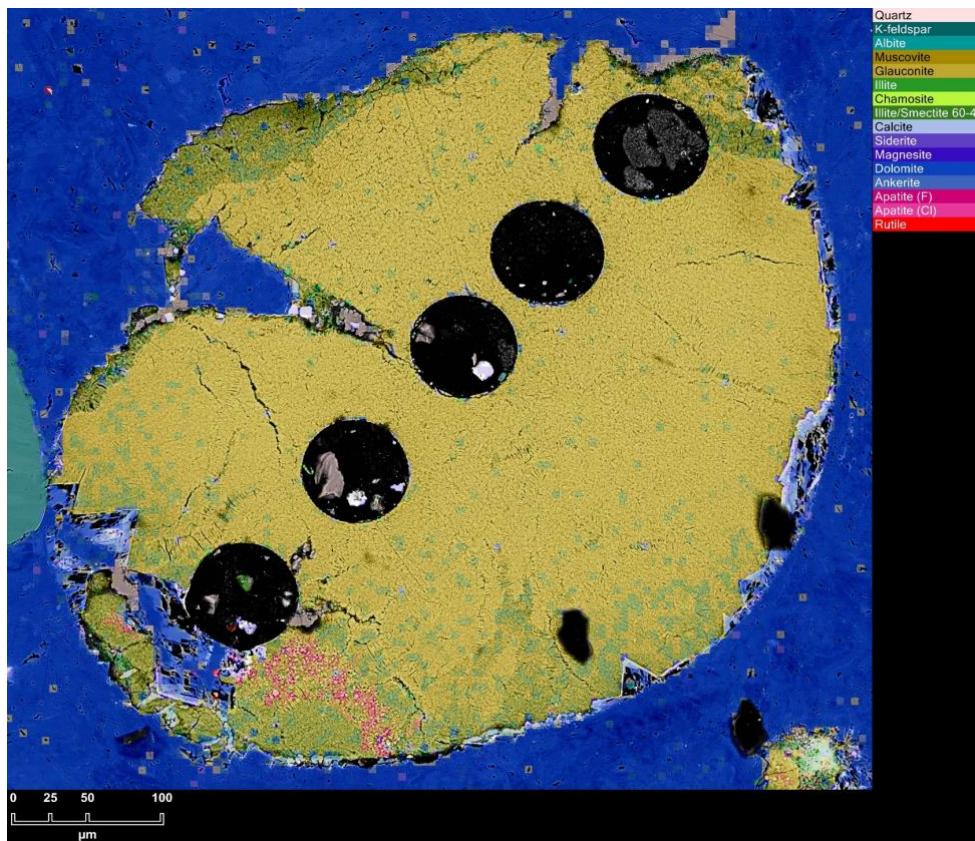
Figure 9: A profile with LA spots across a single glauconite grain (brown) enclosed in dolomite (blue) that does not show evidence for significant replacement by apatite (pink). Sample G2 from Vindhyan Basin, India.

The chemical composition of glauconite could play a significant role on the appearance

colour in Nanomin images. E.g., the glauconite grain in the above image seems to be

darker towards the rims (likely due to presence of illite), suggesting that individual

glauconite grains can have different compositions/mineralogies and thus can yield

different Rb/Sr ages. The back scattered images obtained by the FEI Teneo emission

Scanning Electron Microscope (SEM) show that the zonation on the glauconite grain is

a function of the chemical compositions of the glauconite.
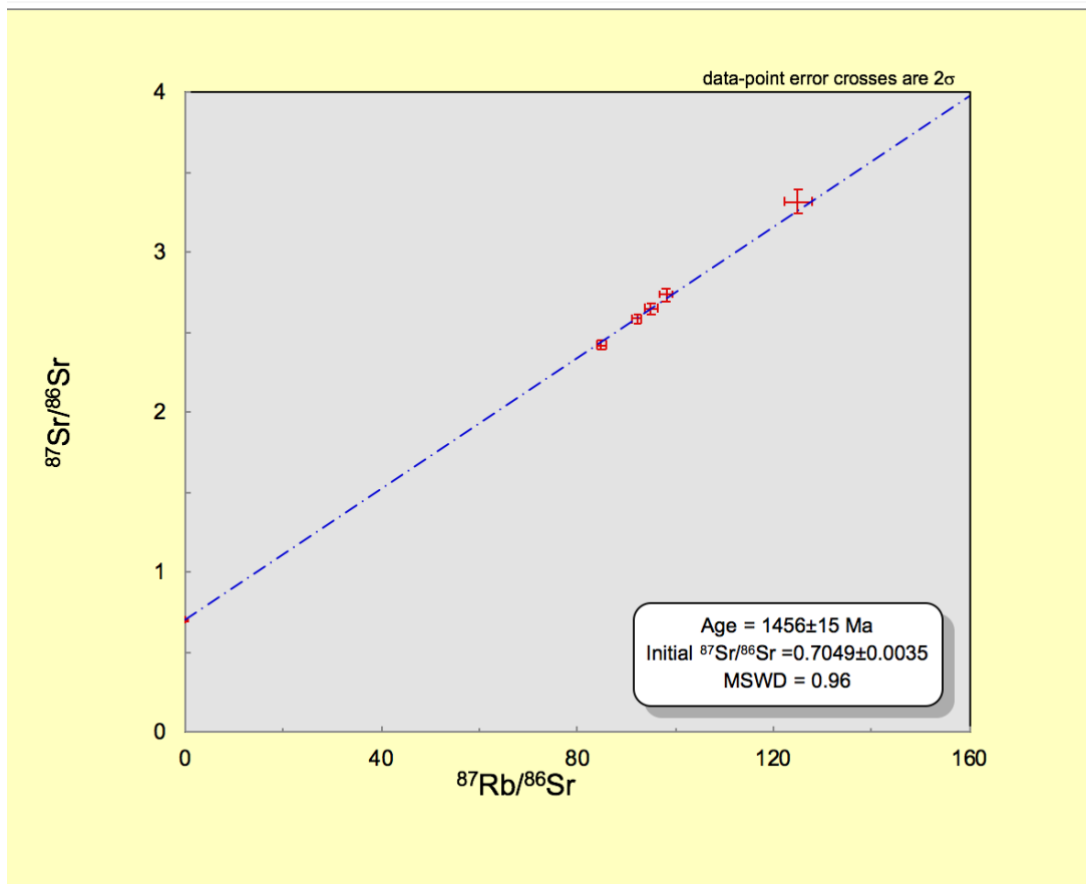
Figure 10: A single-grain Rb/Sr isochrone from sample G2 showing an age of about 1456± 15 Ma (and MSWD <1), using an initial ^{87}Sr/^{86} Sr of 0.705.

Figure 10 shows a profile through the glauconite grain from sample G2, from Semri

Group in Vindhyan Basin. Note that all the laser spots- except for the last spot at the

bottom left corner (which is set initial ^{87}Sr/^{86}Sr of 0.705), were collected from the

glauconite grain that does not show alteration of replacement by apatite or illite.

The results for this single-grain glauconite from sample G2 are excellent and superior to

multiple grain analysis, as the MSWD for single glauconite Rb/Sr age is <1, suggesting

that all points are within analytical errors overlapping or fitting well with the

constructed ischrone, giving a robust age of 1456 ± 15 Ma (with MSWD of ~1)

SAMPLE G6 – VINDHYAN BASIN (SEMRI GROUP, CHITRAKOOT FORMATION):
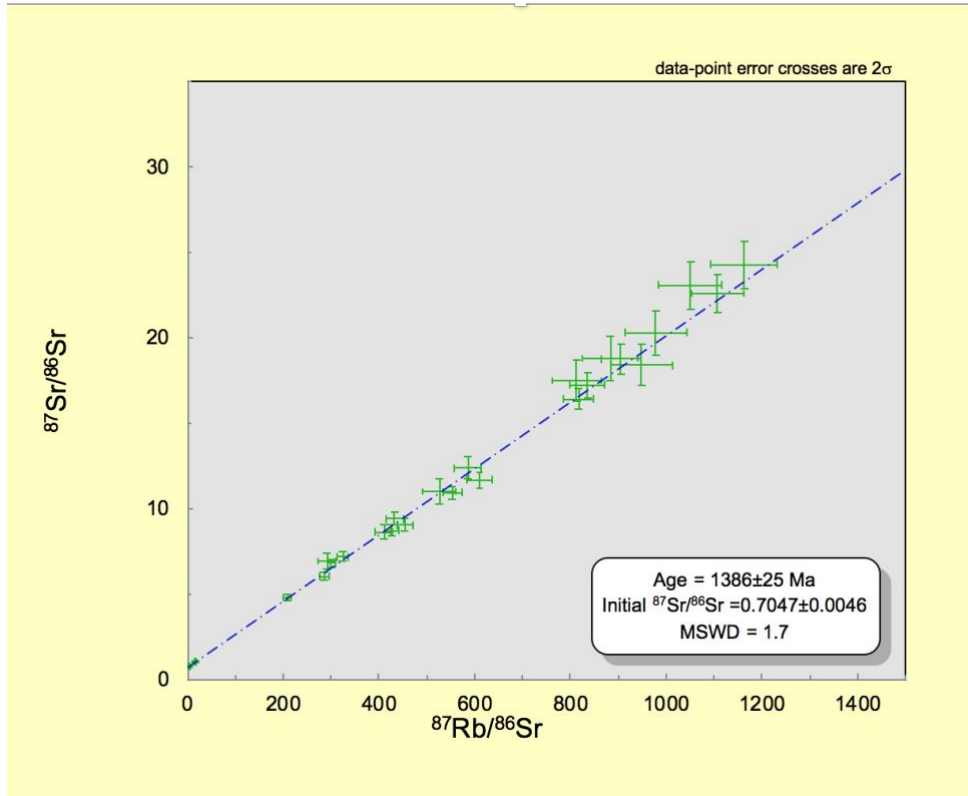
Figure 11: A sample G6 Isochron showing an age of about 1386 25 Ma using an initial 87Sr/86 Sr of 0.705.

The isochron (Figure 16) for the sample yielded an age of 1386± 25 Ma (and MSWD

value of 1.7) using an initial $^{87}Sr/^{86}$ Sr of 0.705.

The data points and the isochron show however larger errors of (± 25 Ma). The MSWD

value is greater than one which means that the variation from the regression of the data

points is likely caused by a geological factor (White 2013). But on the other hand, the

data points are not varied that much from the line, they show a quite good fit and

correlated pattern.
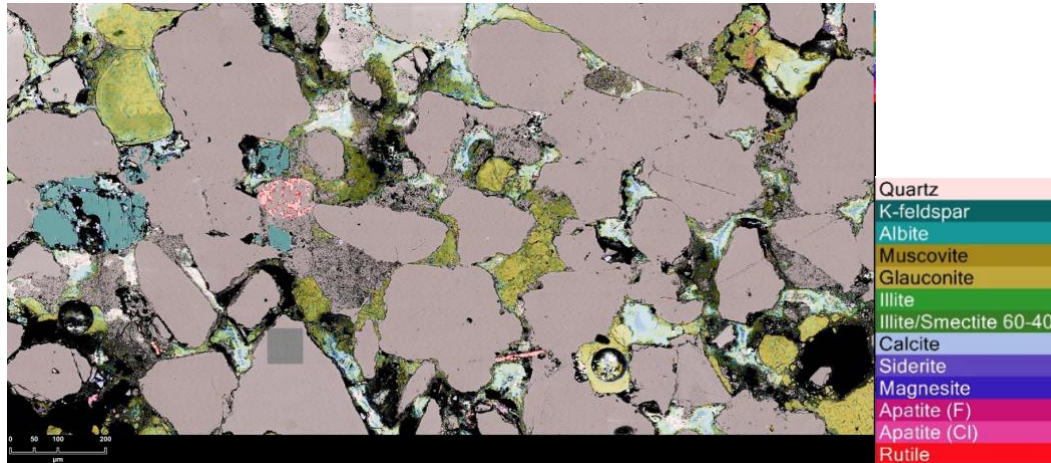
Figure 12: A mineral map of the sample G6 showing the mineralogy of the sample in different colours as well as the laser spots. Note that the laser spot on the right southern part hitting the glauconite where the spot on the left side hits mixed minerals.

By looking at the mineral composition shown on figure (12), the sample is mostly

consisting of quartz (grey). The glauconite is not abundant in this sample, be noticed

that the laser points shown on the mineral map hitting the glauconite. The left laser

point hits the glauconite but also with a mix of mineral which could be a source of noise

in data from this particular and relatively glauconite-poor sample.
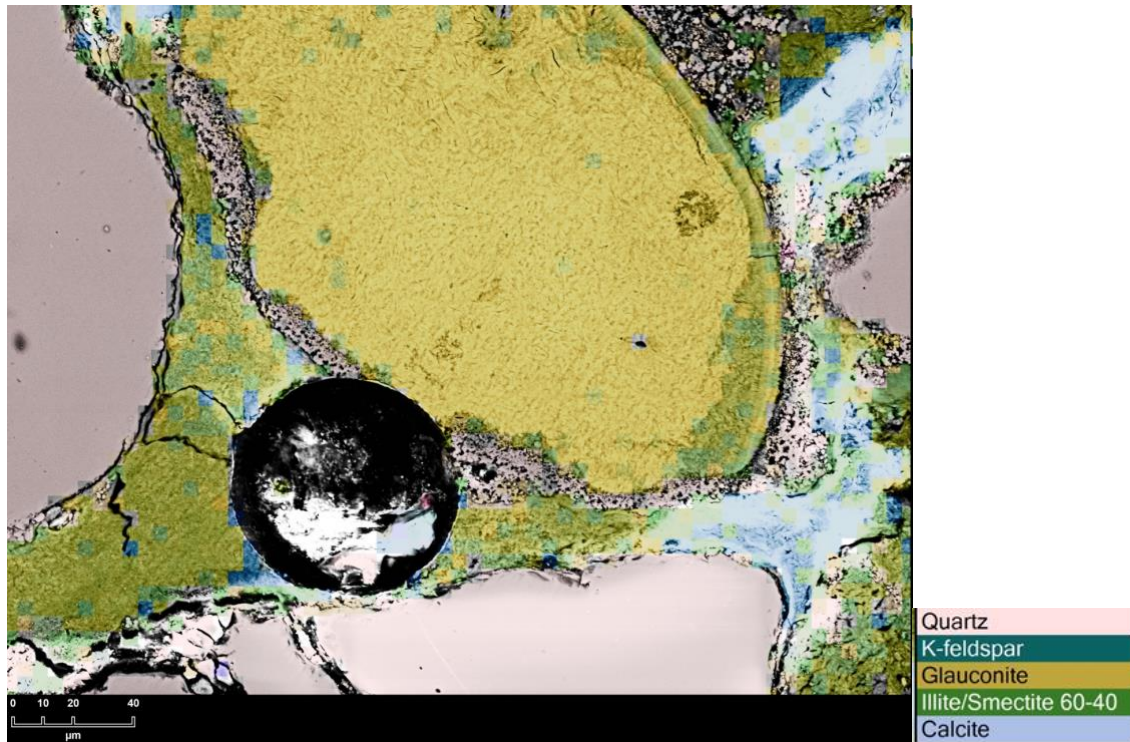
Figure 13: A mineral map showing the laser spot in sample G6. Note that the spot is located between glauconite, calcite and K-feldspar suggesting a need of correction by excluding these points in the Rb-Sr calculations of glauconite.

Figure 13 shows another example of a problematic laser spot located between glauconite, calcite and K-feldspar minerals. These two examples could explain the larger errors associated with this sample and constructed isochron.

Nevertheless, the data from sample G6 shows an expected mid-Proterozoic age of of 1386± 25 Ma (although with larger errors).

SAMPLE G8 - CHHATTISGARH BASIN (RAIPUR GROUP)
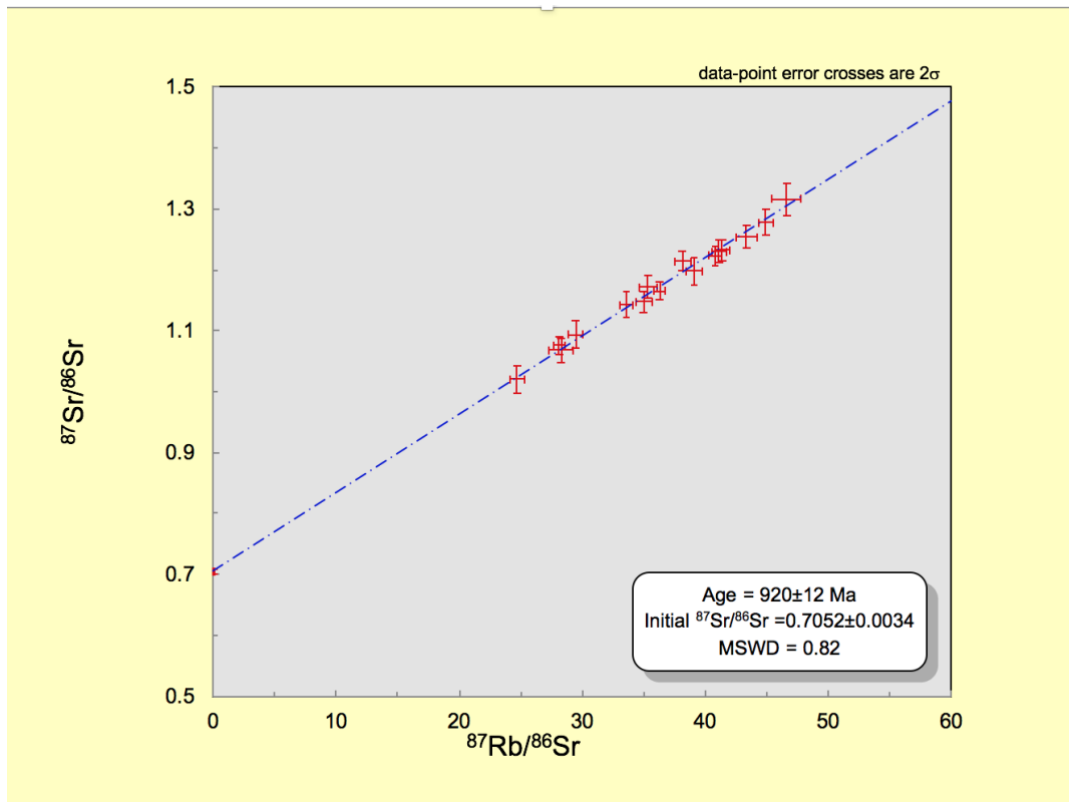
Figure 14: A sample G8 Isochron showing an age of about 920☐ 12 Ma using an initial 87Sr/86Sr of 0.705.

The isochron (Figure 14) for the sample G8 yielded an age of 920± 12 Ma (MSWD

value of 0.82) using an initial $^{87}Sr/^{86}$ Sr of 0.705. The MSWD value is less than one

(0.82), which means that the deviation from the isochron is less than or equal to the

expected associated analytical errors (White 2013). There is also no evidence of

possible separate glauconite populations as the data points are spread along the line.
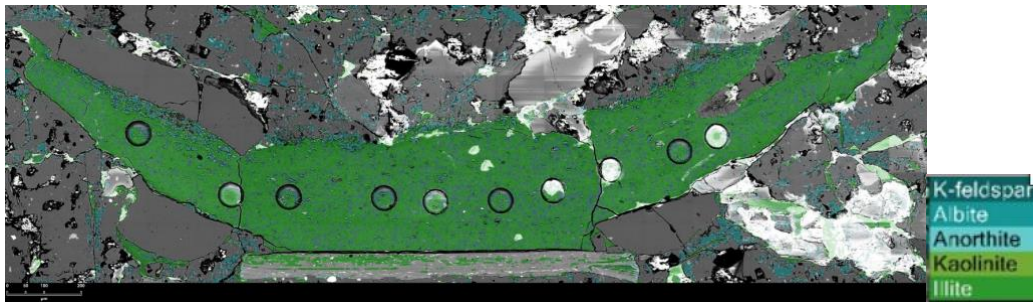
Figure 15: A Mineral map of the sample G8 showing the mineralogy of the sample which is mostly illite and k-feldspar. the laser spots through the profile of illite suggesting a need of correction by excluding these points in the Rb-Sr calculations of glauconite.

Imortantly, Figure (15) shows the complex mineralogy of the sample G8 which is obviously composted of multiple clay mineral phases and not just glauconite. In fact, glauconite is minor phase here and dominant minerals in this sample are illite and K-feldspar, and quartz; plus variable portions of other clay minerals such as kaolinite, clinochlore. The figure above shows a profile through the illite grain, which was originally presumed to be glauconite due to its greenish appearance.
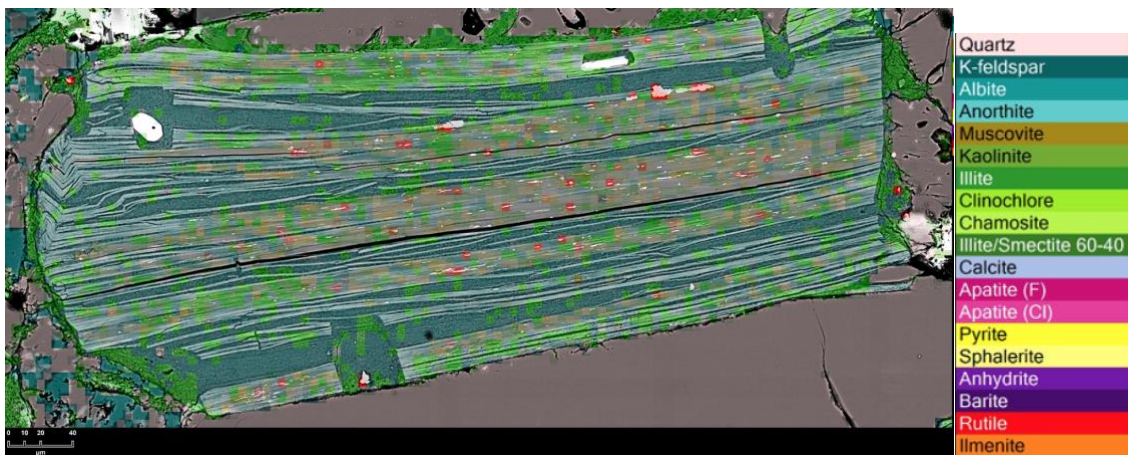

Figure 16: A Mineral map of the sample G8 showing the mineralogy of the sample. Bands appear to alternate between K-feldspar (dominant mineral), illite, muscovite, some rutile (red).

Figure (16) shows the mineralogy of the sample G8 appearing have bands that alternate between K-feldspar, illite, muscovite and some rutile each with different colour as shown on the legend. K-feldspar is the dominant mineral in this sample.

Laser spots were randomly distributed as profiles along the sample since it was really

hard to identify target greenish minerals, which were originally though to be glauconite.
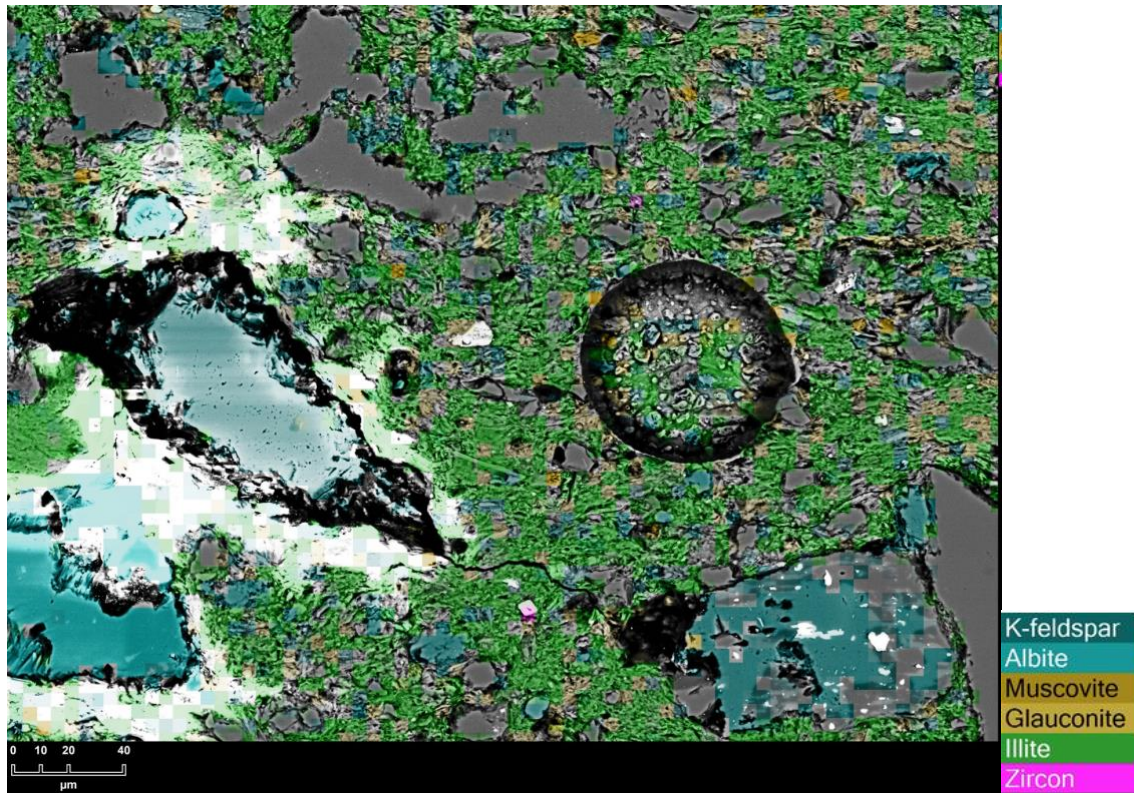
Figure 17: A mineral map image of the sample G8 showing a Complex matrix of illite, quartz, muscovite kaolinite, glauconite, albite and anorthite.

In Figure (17), a laser spot is targeting a complex matrix of minerals including illite,

quartz, muscovite kaolinite, glauconite, albite and anorthite. The bright white area

represents the charging areas due to poor carbon coating. The abundance of glauconite

is very low in this sample as shown on the above micro-scale mineral map.

Despite the mixed mineralogy of this complex sample G8 from Chhatisgarh Basin

(Raipur Group), the acquired Rb/Sr isochron gave an age of 920 ± 12 Ma (MSWD value

of 0.82), which are close to expected published Proterozoic age for these sedimentary

units (Ram, 2012).

SAMPLE G10- KUTCH BASIN
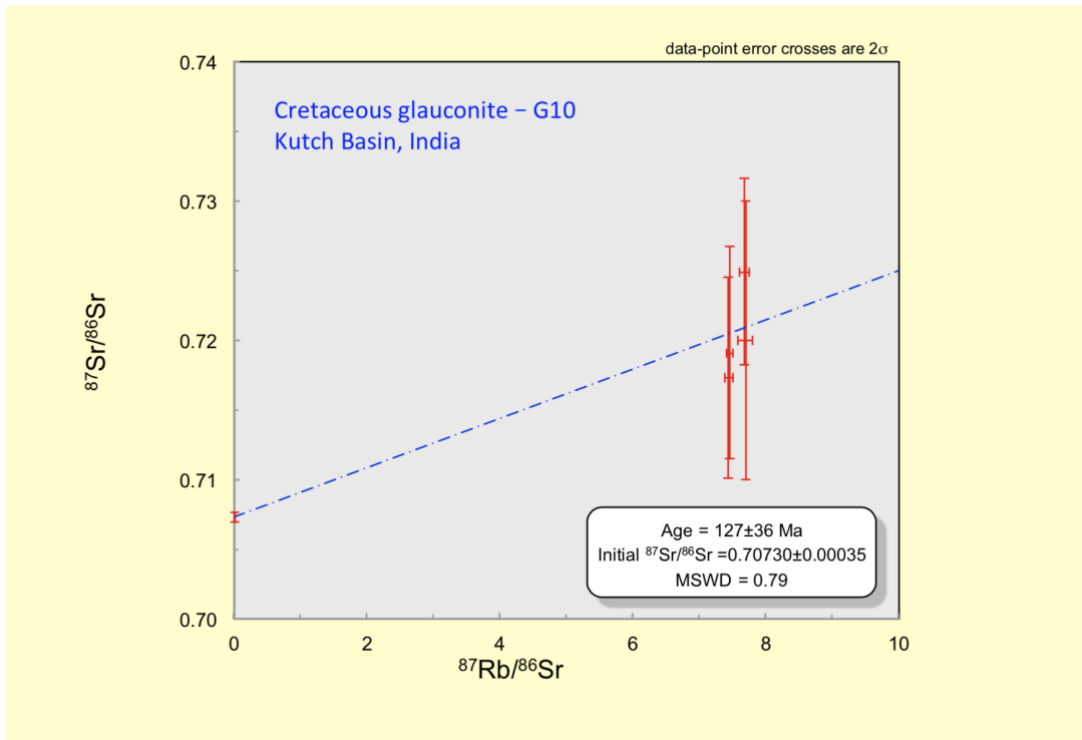
Figure 18: A sample G10 Isochron showing an age of about 127± 36 Ma using an initial ^{87}Sr/^{86} Sr of 0.7073 for Cretaceous seawater.

The isochron Figure (18) for the sample G10 shows an expected Cretaceous age of 127± 36 Ma using an initial ^{87}Sr/^{86} Sr of 0.7073, and MSWD value of 0.79. The data points on the isochron show however large errors of ± 36 Ma, which the biggest amongst the analysed samples so far. This is due to young age of the sample and minimum radiogenic ingrowth of ^{87}Sr, and thus limited range of ^{87}Sr/^{86}Sr variation in this sample. The sample G10 has not been coated and analysed on the FEI Teneo emission Scanning Electron Microscope (SEM), so there is no mineral map available for this sample.

DISCUSSION

SAMPLE G2 - VINDHYAN BASIN, SEMRI GROUP

In the sample analysed, the formation of glauconite does not occur as a single, continuous layer (figure 19). Two glauconite layers are observed separated by a carbonate layer in the middle with the presence of apatite on both layers. When the two layers were treated as a single layer, the results show an isochron with two groups of clustering points (figure 7). Thus, it is not surprising that the MSWD value of this sample was high (5.2) suggesting that the variations are caused by external factors such as geological processes and/or presence of multiple glauconite populations.
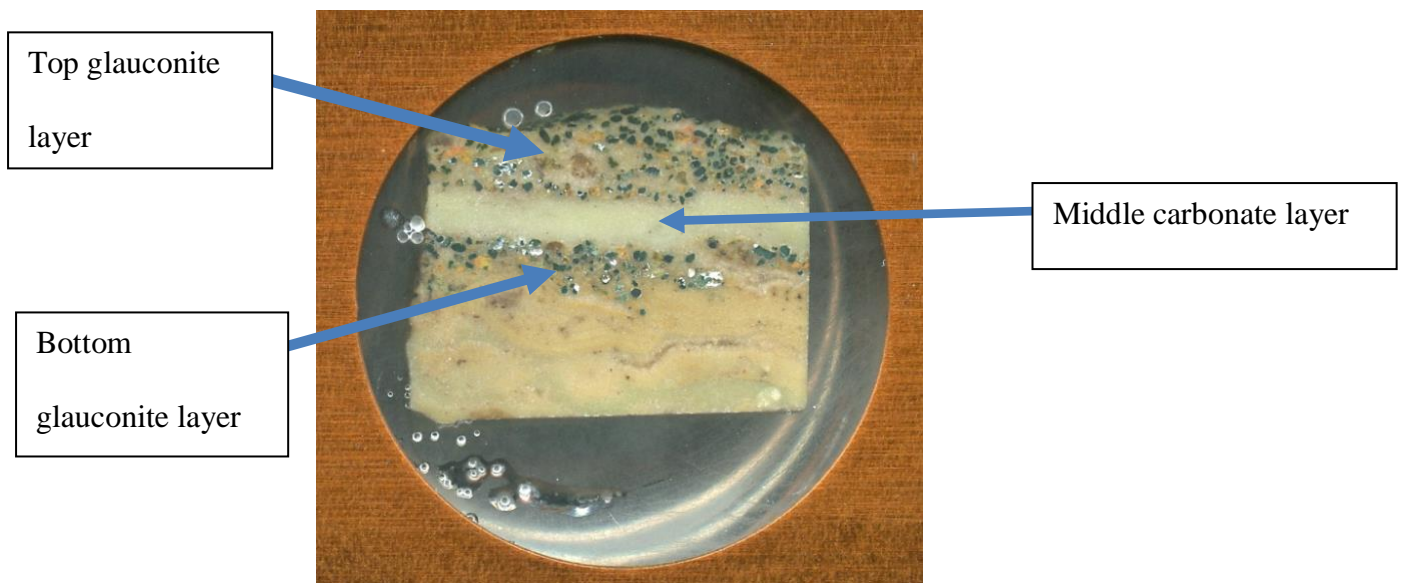

Figure 19: A an image of G2 sample showing two distinct layers of glauconites.

In order to confirm whether these variations are caused by multiple populations or not, an isochrone for each layer (top and bottom) was constructed (figures 20 and 21).
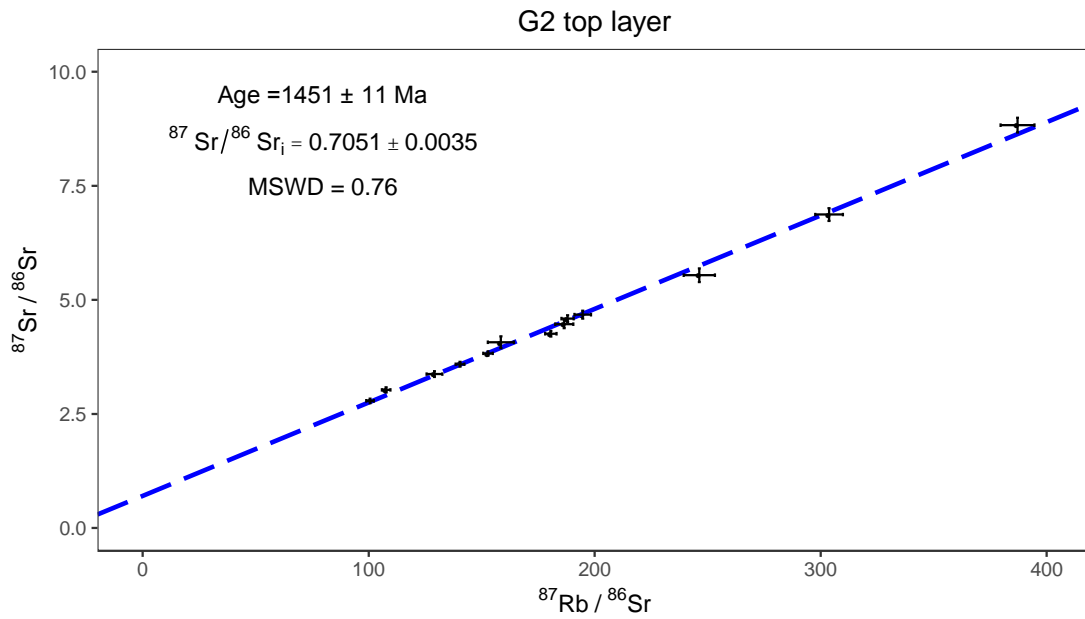
Figure 20: A sample G2 top layer isochron showing an age of 1451± 11 Ma using an initial 87Sr/86 Sr of 0.705.
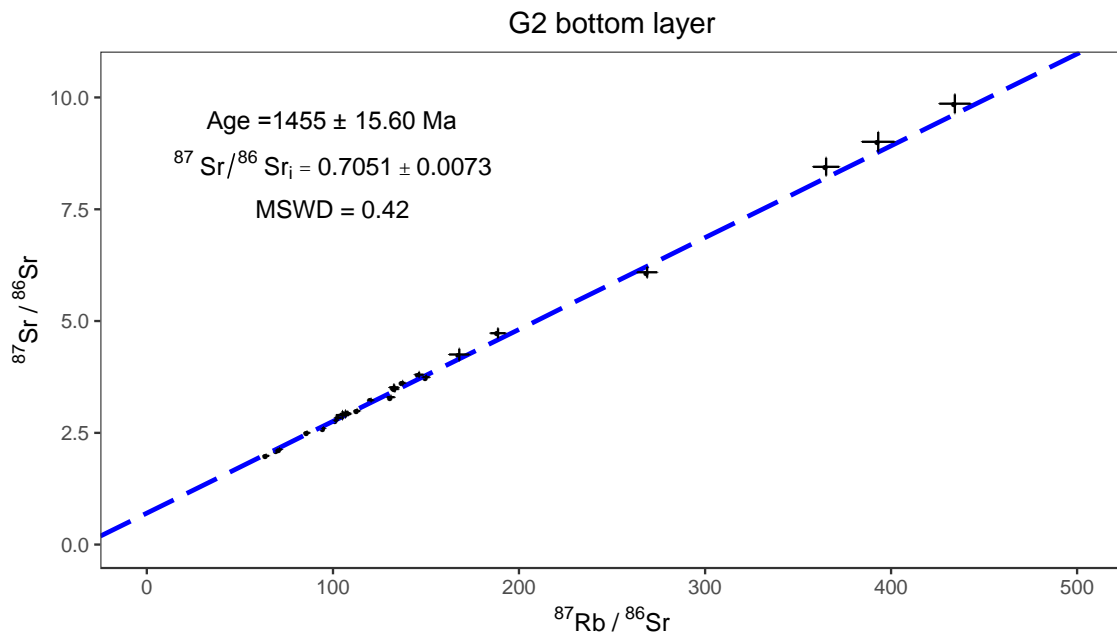

Figure 21: A sample G2 bottom layer isochron showing an age of 1455± 15.60 Ma using an initial 87Sr/86 Sr of 0.705.

The two constructed isochrones from distinct glauconite layers in the sample G2 show within the errors basically the identical ages (~1451 and ~1455 Ma). These results, thus

excludes the idea of having two different populations within the same layer as both layers are giving the same age, however, grains from such distinct populations can still be randomly distributed within the sample and the above two layers.

In addition, the presence of apatite suggests alternative possible scenarios, one of them is that the bulk sample and the Rb/Sr system in glauconites have been partly or completely reset due to younger tectonic processes, thermal events or fluid migration. The Proterozoic tectonics are characterised by the assembly and growth of two supercontinents, when most of the earth's landmasses were joined together. Namely, Columbia/Nuna in the Paleoproterozoic and Rodinia in Late Mesoproterozoic. The orogenic events between the two supercontinent formation events in the time period 1.75 to 1.5 Ga were widespread in different mobile belts around the world. In the Indian peninsula, evidence of several tectono-thermal events in the Proterozoic is present. One of the oldest events is the Paleoproterozoic to Early Mesoproterzoic Tectonic Event (ca. 1800—1500 Ma). These tectonic events are then followed by the ca. 1300—900 Ma Late Mesoproterozoic and "Grenvillian" Tectonothermal Event and the ca. 650—500 Ma Neoproterozoic Pan-African Tectonothermal Event (Bhowmik 2012).

Apatite could be related to one of those events which suggests a further study by doing a U-Pb dating of apatite. By comparing the date of apatite with the events that happened in the Proterozoic, the story of the glauconite can be revealed. Also, knowing the formation temperature of the carbonate layer or dolomite matrix from this sample with glauconite layers (e.g. via clumped isotope analysis of carbonates) could help revealing the meaning of the measured Rb/Sr ages (~1456 ± 15 Ma) and if these indeed reflect primary depositional ages or some later stage diagenetic processes when RbSr system could have been reset.

Kumar et al. 2001 reported ages of identical glauconites from Semri group (Vindhyan

Basin) using Rb-Sr dating of bulk samples via TIMS. The mean age of the glauconite in

the above study was 1475 ±19 Ma which matches well with the acquired ages using in-

situ Rb-Sr dating via LA-ICP MS/MS. As shown on figure 22, the TIMS-based ages

from Kumar et al.2001 match well the in-situ RbSr age generated by this study.
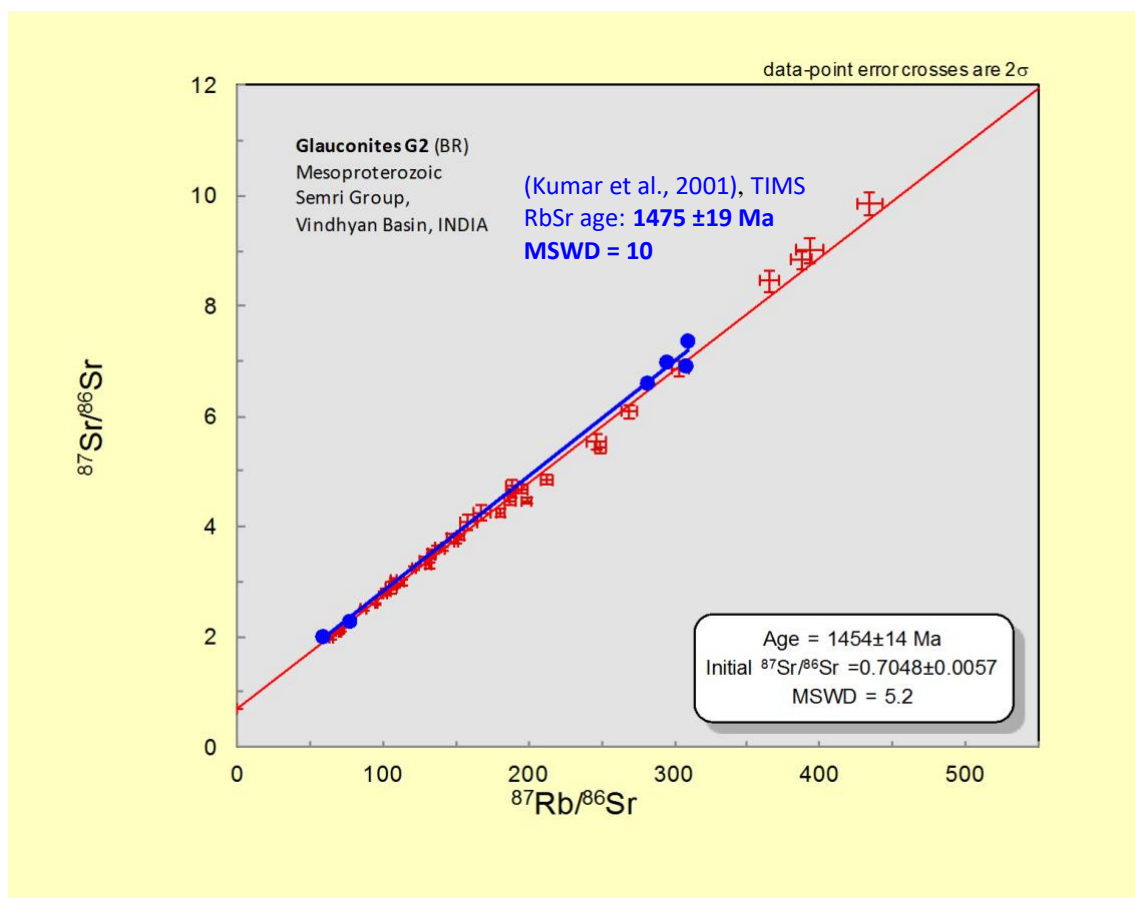
Figure 22: Comparison of in-situ RbSr data from sample G2 (red isochron – this study) with published TIMS-based RbSr age on equivalent glauconite samples from Semri Group (Vindhyan Basin) reported by Kumar et al. 2001 (blue isochrone with age of 1475± 19 Ma).

By comparing the isochrones for both studies, similar pattern of data scattering is

observed, suggesting that indeed at least two glauconite populations (older and younger)

are present in Semri Group (see Kumar et al. 2001).

34

SAMPLE G8 - CHHATTISGARH BASIN (RAIPUR GROUP)

In this sample, the mineralogy was mostly consisting of K-feldspar and illite. The abundance of glauconite was very low. The resulted in-situ Rb/Sr age for this sample was 920± 12 Ma (MSWD value of 0.82) and thus slightly younger than the age found by Bickford et al. 2011 which was 993±8 Ma (~70 Ma gap) using U-Pb SHRIMP method for Raipur Group (Kumar et al. 2001). The younger age thus likely reflect the timing of formation of these later diagenetic mineral assemblages (illite, K-feldspar), which thus occurred much later after sediment deposition.

SAMPLE G10- KUTCH BASIN

This sample was the youngest among all the samples analysed. It yielded in-situ RbSr age of 127 ± 36 Ma which is within the expected Cretaceous age for these glauconite assemblages. Specifically, Rathore et al. (1999) and Bansal et al. (2017) reported K-Ar ages in the range of 104 to 108 Ma, and 113 to 125 Ma, respectively. To apply Rb-Sr dating method on glauconite, the glauconite by itself has to be mature (having enough K_2O) to produce a reliable age. In this sample, the noise and the large errors are caused by the immaturity of the glauconite sample and small radiogenic ingrowth of ^{87}Sr from ^{87}Rb decay (due to young age and extremely long half-life of ~49 Ga) which makes the Rb/Sr system not suitable for dating of young samples (Rink & Thompson, 2015).

CONCLUSIONS

Mature Mid-Proterozoic glauconites from the Vinhyan Basin (Semri Group) used in this study gave in-situ RbSr ages that are within the range of the expected ages for Semri Group deposits suggested by other published studies. Mineralogical and chemical compositions (K_2O contents) of glauconite have to be carefully characterised to validate the use of in-situ Rb-Sr isotope dating method for glauconites. A single-grain Rb/Sr profile isochrons are possible with in-situ Rb/Sr dating technique using LA-ICP MS/MS, but these analyses need to be carefully navigated with detail mineral maps of samples (i.e., the back scattered images BSE obtained by the FEI Teneo emission Scanning Electron Microscope SEM). However, young and immature glauconites will result in uncertain and noisy Rb-Sr ages (as tested on Cretaceous samples from the Kutch Basin), and these are due to a small range of measurable variability in $^{87}Sr/^{86}Sr$ and $^{87}Rb/^{86}Sr$ ratios found in these young glauconite samples.

REFERENCES

Baldermann, A, Dietzel, M, Mavromatis, V, Mittermayr, F, N. Warr, L, & Wemmer, K 2017. The role of Fe on the formation and diagenesis of interstratified glauconite-smectite and illite-smectite: A case study of Upper Cretaceous shallow-water carbonates, *Chemical Geology* 453, pp. 21–34.

Banerjee, S, Nansal, U, & Thorat, A.V 2016. A review on palaeogeographic implications and temporal variation in glaucony composition, *Journal of Palaeocenography*, Vol. 5, p. 43-71.

Bansal, U, Banerjee, S, Pande, K, Arora, A, & S.S. Meena 2017. The distinctive compositional evolution of glauconite in the Cretaceous Ukra Hill Member (Kutch basin, India) and its implications, *Marine and Petroleum Geology* 82, pp. 97-117.

Bhowmik, S. K., Chattopadhyay, A,Gupta, & S. Dasgupta, S 2012. Proterozoic Tectonic: An Indian perspective, *Indian National Science Academy Journal*, 78(3), pp. 385-391.

Chakraborty, P, Saha, S, & Das, P 2015. Geology of Mesoproterozoic Chhattisgarh Basin, Central India: current status and future goals, *Geological Society London Memoirs* 43(1), pp. 185–205.

Derkowski , A, Środoń , J, Franus , W, Uhlík , P , Banaś, M, Zieliński, G , Čaplovičová, M , & Franus, M 2009. PARTIAL DISSOLUTION OF GLAUCONITIC SAMPLES: IMPLICATIONS FOR THE METHODOLOGY OF K-Ar AND Rb-Sr DATING, *Clays and Clay Minerals* 57 (5), pp. 531-554.

Directorate General Of Hydrocarbon 2017. The Vindhyan basin, *Directorate General Of Hydrocarbon*, pp. 1-5.

Falster, G, Tyler, J, Grant, K, Tibby, J, Turney, C, Loehr, S, Jacobsen, G, & A. Kershaw P 2018. Millennial-scale variability in south-east Australian hydro climate between 30,000 and 10,000 years ago, *Quaternary Science Reviews* 192, pp.106-122.

Hegab, O, Ahmed, G, & El-wahed A 2016. Origin of the glauconite from the Middle Eocene, Qarara Formation, Egypt, *Journal of African Earth Sciences*12, pp. 21-28.

Hogmalm, K. J., Zack, T., Karlsson, A.K. O., Sjoqvit, A. S., & Garbe-Schonberg, D 2017. In situ Rb—Sr and K—Ca dating by LA-ICP-MS/MS: an evaluation of N 2 O and SF 6 as reaction gases, *Journal of Analytical Atomic Spectrometry*, 32(2), pp. 305-313.

Hower, J 1961. Some factors concerning the nature and origin of glauconite. *Amer. Min* 46, pp. 313-334.

Jensen, L 2017, A novel in-situ method for Rubidium Strontium (Rb-Sr) dating of igneous rocks and minerals, Lisa (Honours Thesis 2017), University of Adelaide.

M. Rahman, H, Kennedy, M, Loehr, S, N. Dewhurst, D, Sherwood, N, Yang, S, & Horsfield, B 2018. The influence of shale depositional fabric on the kinetics of hydrocarbon generation through control of mineral surface contact area on clay catalysis, *Geochimica et Cosmochimica Acta* 220, pp. 429–448.

National Data Repository 2015. Kutch Basin, 2015, viewed 15 October 2018, < https://www.ndrdgh.gov.in/NDR/?page_id=742>.

Ram, J 2012. Neoproterozoic successions in Peninsular India and their hydrocarbon prospectivity. *Geological Society of London, Special Publications*, Vol. 366, DOI: 10.1144/SP366.4.

Rathore, S.S, Prabhu, B.N, Vijan, A.R, Vic, K.C, & Misra, K.N 1999. K-Ar age of Ukra glauconites from the Kutch Basin, India, *Earth Planet Science* 108, no.1, pp. 49-55.

Rink, W. J., & Thompson, J. W. (2015), *Encyclopedia of scientific dating methods*. doi: 10.1007/978- 94-007-6304-3.

Shields, G, & Veizer, J 2002. Precambrian marine carbonate isotope database: Version 1.1, *AGU and The Geochemical Society*, no. 6, vol. 3, pp. 1-12.

Technologies, A. 2016. Agilent 8900 Triple Quadrupole ICP-MS Technical Overview, *Agilent Technologies*, (5991-6990EN), pp. 1-10.

Villa, I., De Bièvre, P., Holden, N., & Renne, P. (2015). IUPAC-IUGS recommendation on the half-life of 87Rb. *Geochim et cosmochimica Acta* 164, pp. 382-385.

White W. M 2013. Basics Of Radioactive Isotope Geochemistry, *Isotope Geochemistry*, 2013, viewed on 13 October 2018, < http://www.geo.cornell.edu/geology/classes/Geo656/656notes13/IsotopeGeochemistry%20Chapter2.pdf >.

Zack, T, & Hogmalm, J 2016. Laser ablation Rb/Sr dating by online chemical separation of Rb and Sr in an oxygen-filled reaction cell, *Chemical geology* 473, pp. 120-133.

APPENDIX A: RAW DATA AND PROFILES FOR ALL THE SAMPLES USED FOR LA-QQQ:

	Source file	StdCorr_Rb87_Sr86s	StdCorr_Rb87_Sr86s_Int2SE	StdCorr_Sr87s_Sr86s	StdCorr_Sr87s_Sr86s_Int2SE
G_NIST610_1	NIST 610 - 11	2.0342	0.008	0.7107	0.0016
G_NIST610_2	NIST 610 - 12	2.0247	0.0074	0.7085	0.0018
G_NIST610_3	NIST 610 - 13	2.0453	0.0076	0.7096	0.0019
G_NIST610_4	NIST 610 - 14	2.0304	0.0075	0.7095	0.0016
G_NIST610_5	NIST 610 - 15	2.0385	0.0076	0.7093	0.0018
G_NIST610_6	NIST 610 - 16	2.0381	0.0074	0.7105	0.0016
G_NIST610_7	NIST 610 - 17	2.0454	0.0075	0.7101	0.0018
G_NIST610_8	NIST 610 - 18	2.0363	0.0072	0.7115	0.0016
G_NIST610_9	NIST 610 - 19	2.0502	0.0075	0.7099	0.0017
G_NIST610_10	NIST 610 - 20	2.0475	0.0068	0.7103	0.0016
G_NIST610_11	NIST 610 - 21	2.0482	0.0073	0.7087	0.0018
G_NIST610_12	NIST 610 - 22	2.0451	0.0081	0.7099	0.0014
G_NIST610_13	NIST 610 - 23	2.0426	0.0066	0.7097	0.0017
G_NIST610_14	NIST 610 - 24	2.0381	0.0073	0.7111	0.0015
G_NIST610_15	NIST 610 - 25	2.0449	0.0071	0.7097	0.0017
G_NIST610_16	NIST 610 - 26	2.0385	0.0069	0.7094	0.0017
G_NIST610_17	NIST 610 - 27	2.0418	0.0078	0.7085	0.0018
G_NIST610_18	NIST 610 - 28	2.0432	0.008	0.7105	0.0018
G_NIST610_19	NIST 610 - 29	2.0327	0.0075	0.7102	0.0015
G_NIST610_20	NIST 610 - 30	2.0324	0.0068	0.71	0.002
G_NIST610_21	NIST 610 - 31	2.0323	0.0079	0.7106	0.0017
G_NIST610_22	NIST 610 - 32	2.0374	0.007	0.7106	0.0017
G_NIST610_23	NIST 610 - 33	2.0324	0.0077	0.7097	0.0018
G_NIST610_24	NIST 610 - 34	2.0281	0.0081	0.7107	0.0018
M_MDCmica_1	MDC - 16	39.37	0.36	1.0249	0.0072
M_MDCmica_2	MDC - 17	39.29	0.39	1.0201	0.0066
M_MDCmica_3	MDC - 18	39.78	0.44	1.0356	0.0075
M_MDCmica_4	MDC - 19	39.62	0.49	1.0256	0.0065
M_MDCmica_5	MDC - 20	39.65	0.47	1.0364	0.0063
M_MDCmica_6	MDC - 21	39.71	0.49	1.0209	0.0079
M_MDCmica_7	MDC - 22	39.44	0.5	1.0308	0.0062
M_MDCmica_8	MDC - 23	39.63	0.45	1.0283	0.006
M_MDCmica_9	MDC - 24	40.09	0.46	1.0396	0.0065
M_MDCmica_10	MDC - 25	39.81	0.49	1.028	0.0073
M_MDCmica_11	MDC - 26	40.03	0.49	1.0216	0.0071
M_MDCmica_12	MDC - 27	40.29	0.45	1.0311	0.0081
M_MDCmica_13	MDC - 28	40.56	0.49	1.0367	0.0079
M_MDCmica_14	MDC - 29	40.69	0.46	1.0378	0.0064
M_MDCmica_15	MDC - 30	40.65	0.51	1.0328	0.0071
M_MDCmica_16	MDC - 31	40.9	0.55	1.0281	0.0065

M_MDCmica_17	MDC - 32	40.91	0.6	1.0383	0.0081
M_MDCmica_18	MDC - 33	40.95	0.46	1.034	0.0073
M_MDCmica_19	MDC - 34	41.37	0.5	1.031	0.0066
M_MDCmica_20	MDC - 35	40.95	0.51	1.0339	0.0081
M_MDCmica_21	MDC - 36	40.76	0.47	1.0401	0.0068
M_MDCmica_22	MDC - 37	40.86	0.48	1.0446	0.0078
M_MDCmica_23	MDC - 38	41.02	0.5	1.0353	0.0079
M_MDCmica_24	MDC - 39	41.05	0.53	1.0308	0.0067
M_MDCmica_25	MDC - 40	40.94	0.53	1.0394	0.0068
M_MDCmica_26	MDC - 41	41.42	0.44	1.0346	0.0072
M_MDCmica_27	MDC - 42	40.88	0.5	1.0322	0.0064
M_MDCmica_28	MDC - 43	40.93	0.46	1.0292	0.0065
M_MDCmica_29	MDC - 44	41.17	0.5	1.0393	0.0068
M_MDCmica_30	MDC - 45	40.66	0.51	1.0367	0.0074
M_MDCmica_31	MDC - 46	41.47	0.52	1.0353	0.0073
M_MDCmica_32	MDC - 47	41.87	0.55	1.0427	0.0063
M_MDCmica_33	MDC - 48	41.46	0.5	1.0376	0.0069
M_MDCmica_34	MDC - 49	39.38	0.46	1.0242	0.0071
M_MDCmica_35	MDC - 50	39.91	0.42	1.031	0.0072
M_MDCmica_36	MDC - 51	40.28	0.45	1.0338	0.0072
M_MicaMg_1	Mica Mg - 16	160.9	1.6	1.869	0.016
M_MicaMg_2	Mica Mg - 17	155	1.3	1.841	0.015
M_MicaMg_3	Mica Mg - 18	153.2	1.4	1.861	0.014
M_MicaMg_4	Mica Mg - 19	155.3	1.6	1.858	0.013
M_MicaMg_5	Mica Mg - 20	153.7	1.4	1.843	0.015
M_MicaMg_6	Mica Mg - 21	159	1.5	1.861	0.019
M_MicaMg_7	Mica Mg - 22	157.5	1.3	1.867	0.016
M_MicaMg_8	Mica Mg - 23	155.6	1.5	1.862	0.018
M_MicaMg_9	Mica Mg - 24	156.4	1.8	1.845	0.016
M_MicaMg_10	Mica Mg - 25	157.6	1.7	1.84	0.015
M_MicaMg_11	Mica Mg - 26	154.4	1.3	1.844	0.015
M_MicaMg_12	Mica Mg - 27	155.4	1.4	1.839	0.016
M_MicaMg_13	Mica Mg - 28	154.3	1.5	1.859	0.015
M_MicaMg_14	Mica Mg - 29	148.8	1.6	1.838	0.015
M_MicaMg_15	Mica Mg - 30	153.8	1.4	1.842	0.017
M_MicaMg_16	Mica Mg - 31	158.4	1.6	1.873	0.017
M_MicaMg_17	Mica Mg - 32	157.3	1.5	1.856	0.016
M_MicaMg_18	Mica Mg - 33	157.1	1.3	1.861	0.014
M_MicaMg_19	Mica Mg - 34	153	1.5	1.844	0.015
M_MicaMg_20	Mica Mg - 35	154.1	1.3	1.85	0.015
M_MicaMg_21	Mica Mg - 36	153.6	1.4	1.849	0.016

M_MicaMg_22	Mica Mg - 37	153.8	1.5	1.865	0.019
M_MicaMg_23	Mica Mg - 38	149.5	1.1	1.852	0.016
M_MicaMg_24	Mica Mg - 39	152.2	2	1.86	0.023
M_MicaMg_25	Mica Mg - 40	153.1	1.2	1.842	0.014
M_MicaMg_26	Mica Mg - 41	153.2	1.2	1.852	0.016
M_MicaMg_27	Mica Mg - 42	155.3	1.5	1.844	0.017
M_MicaMg_28	Mica Mg - 43	154.5	1.5	1.843	0.018
M_MicaMg_29	Mica Mg - 44	154.9	1.6	1.865	0.017
M_MicaMg_30	Mica Mg - 45	155	1.4	1.846	0.018
M_MicaMg_31	Mica Mg - 46	152.6	1.6	1.856	0.019
M_MicaMg_32	Mica Mg - 47	151.5	1.6	1.848	0.013
M_MicaMg_33	Mica Mg - 48	148.4	1.4	1.858	0.015
M_MicaMg_34	Mica Mg - 49	155.4	1.7	1.851	0.014
M_MicaMg_35	Mica Mg - 50	155.8	1.3	1.85	0.016
M_MicaMg_36	Mica Mg - 51	156.1	1.6	1.855	0.015
Output_1_1	Mica Mg - 16	159.5	1.7	1.862	0.015
Output_1_2	Mica Mg - 17	154.7	1.3	1.841	0.014
Output_1_3	Mica Mg - 18	153.5	1.4	1.863	0.014
Output_1_4	NIST 610 - 11	2.0342	0.008	0.7107	0.0016
Output_1_5	NIST 610 - 12	2.0247	0.0074	0.7085	0.0018
Output_1_6	MDC - 16	39.37	0.36	1.0249	0.0072
Output_1_7	MDC - 17	39.86	0.31	1.0219	0.0074
Output_1_8	MDC - 18	40.66	0.33	1.031	0.0082
Output_1_9	BCR - 11	0.3629	0.003	0.706	0.0027
Output_1_10	BCR - 12	0.355	0.0035	0.7051	0.0023
Output_1_11	G8 - 1	41.11	0.62	1.23	0.018
Output_1_12	G8 - 2	44.6	0.89	1.323	0.021
Output_1_13	G8 - 3	38.77	0.53	1.193	0.02
Output_1_14	G8 - 4	64.6	2.2	1.492	0.057
Output_1_15	Mica Mg - 19	155.3	1.6	1.858	0.013
Output_1_16	Mica Mg - 20	153.4	1.3	1.843	0.015
Output_1_17	Mica Mg - 21	158.8	1.5	1.861	0.018
Output_1_18	NIST 610 - 13	2.0453	0.0076	0.7096	0.0019
Output_1_19	NIST 610 - 14	2.0304	0.0075	0.7095	0.0016
Output_1_20	MDC - 19	40.39	0.4	1.0276	0.0075
Output_1_21	MDC - 20	40.4	0.36	1.0354	0.0072
Output_1_22	MDC - 21	40.49	0.34	1.0228	0.0093
Output_1_23	BCR - 13	0.356	0.0031	0.7055	0.003
Output_1_24	BCR - 14	0.353	0.0031	0.7067	0.0029
Output_1_25	G8- 6	24.7	0.61	1.02	0.023
Output_1_26	G8 - 8	35.37	0.43	1.189	0.015

Output_1_27	G8- 9	28.1	0.47	1.076	0.014
Output_1_28	G8 - 11	31.38	0.43	1.136	0.019
Output_1_29	G8- 12	46.6	1.2	1.316	0.027
Output_1_30	G8 - 13	45.5	1.1	1.351	0.022
Output_1_31	G8 - 14	48.3	1	1.289	0.022
Output_1_32	G8 - 15	40.79	0.55	1.223	0.016
Output_1_33	G8 - 16	35.84	0.71	1.228	0.026
Output_1_34	G8 - 17	28.3	1	1.068	0.02
Output_1_35	G8 - 18	39.08	0.71	1.198	0.023
Output_1_36	G8 - 19	34.98	0.63	1.148	0.017
Output_1_37	G8 - 20	41.36	0.6	1.232	0.017
Output_1_38	G8 - 21	27.34	0.52	1.102	0.022
Output_1_39	G8 - 22	38.14	0.65	1.214	0.016
Output_1_40	G8 - 23	29.45	0.54	1.094	0.023
Output_1_41	G8 - 24	44.88	0.61	1.278	0.021
Output_1_42	Mica Mg - 22	157.1	1.3	1.867	0.016
Output_1_43	Mica Mg - 23	154.6	1.6	1.863	0.018
Output_1_44	Mica Mg - 24	156.4	1.8	1.845	0.016
Output_1_45	NIST 610 - 15	2.0385	0.0076	0.7093	0.0018
Output_1_46	NIST 610 - 16	2.0381	0.0074	0.7105	0.0016
Output_1_47	MDC - 22	40.44	0.4	1.0301	0.0072
Output_1_48	MDC - 23	40.35	0.35	1.0271	0.0069
Output_1_49	MDC - 24	40.76	0.35	1.0377	0.0073
Output_1_50	BCR - 15	0.3544	0.0033	0.7042	0.0031
Output_1_51	BCR - 16	0.3498	0.0039	0.7032	0.0029
Output_1_52	AR - 26	43.32	0.82	1.254	0.019
Output_1_53	G8 - 27	35.33	0.74	1.172	0.018
Output_1_54	G8 - 29	33.57	0.55	1.142	0.021
Output_1_55	G8 - 30	36.27	0.5	1.165	0.015
Output_1_56	G8 - 32	32.31	0.59	1.149	0.021
Output_1_57	G8 s - 1	91.2	1.3	1.615	0.025
Output_1_58	G8 s - 2	92.6	1.3	1.639	0.026
Output_1_59	G8 s - 4	73.8	1.6	1.481	0.037
Output_1_60	G8 s - 5	73.5	1	1.442	0.024
Output_1_61	G8 s - 6	91.7	1.6	1.659	0.028
Output_1_62	G8 s - 7	93.9	1.7	1.663	0.031
Output_1_63	G8 s - 8	98.6	1.6	1.702	0.029
Output_1_64	G8 s - 9	78.2	1.3	1.55	0.033
Output_1_65	G8 s - 10	71.5	1.7	1.478	0.028
Output_1_66	G2 - 1	133.3	2.1	3.479	0.056
Output_1_67	Mica Mg - 25	157.6	1.7	1.84	0.015
Output_1_68	Mica Mg - 26	154.6	1.4	1.844	0.015

Output_1_69	Mica Mg - 27	154.9	1.4	1.845	0.015
Output_1_70	NIST 610 - 17	2.0454	0.0075	0.7101	0.0018
Output_1_71	NIST 610 - 18	2.0363	0.0072	0.7115	0.0016
Output_1_72	MDC - 25	39.81	0.49	1.028	0.0073
Output_1_73	MDC - 26	40.03	0.49	1.0216	0.0071
Output_1_74	MDC - 27	40.29	0.45	1.0311	0.0081
Output_1_75	BCR - 17	0.3494	0.0038	0.7046	0.0028
Output_1_76	BCR - 18	0.353	0.0033	0.7058	0.0028
Output_1_77	G2 - 2	146.3	2.4	3.802	0.061
Output_1_78	G2 - 3	132.8	2.5	3.516	0.07
Output_1_79	G2 - 4	137.5	1.5	3.614	0.046
Output_1_80	G2 - 5	105.2	3.5	2.896	0.093
Output_1_81	G2 - 6	106.8	3	2.921	0.077
Output_1_82	G2 - 7	108	1.3	2.94	0.037
Output_1_83	G2 - 8	434.3	8.4	9.86	0.21
Output_1_84	G2 - 9	393.1	8.7	9.01	0.22
Output_1_85	G2 - 10	365.1	7	8.45	0.2
Output_1_86	G2 - 11	268.9	5.4	6.09	0.12
Output_1_87	G2 - 12	113	1.6	2.989	0.045
Output_1_88	G2 - 13	188.7	4.1	4.73	0.11
Output_1_89	G2 - 14	167.9	5.4	4.25	0.13
Output_1_90	G2 - 15	194.7	3.7	4.677	0.087
Output_1_91	G2 - 16	188	2.7	4.59	0.071
Output_1_92	G2 - 17	180.6	2.5	4.257	0.062
Output_1_93	G2 - 18	100.6	1.7	2.787	0.049
Output_1_94	Mica Mg - 28	155.1	1.6	1.854	0.016
Output_1_95	Mica Mg - 29	148.2	1.8	1.825	0.014
Output_1_96	Mica Mg - 30	153.8	1.4	1.838	0.017
Output_1_97	NIST 610 - 19	2.0502	0.0075	0.7099	0.0017
Output_1_98	NIST 610 - 20	2.0475	0.0068	0.7103	0.0016
Output_1_99	MDC - 28	40.56	0.49	1.0367	0.0079
Output_1_100	MDC - 29	40.69	0.46	1.0378	0.0064
Output_1_101	MDC - 30	40.65	0.51	1.0328	0.0071
Output_1_102	BCR - 19	0.3584	0.0037	0.7046	0.0028
Output_1_103	BCR - 20	0.3533	0.0043	0.7056	0.0032
Output_1_104	G2 - 19	158.5	5.8	4.07	0.13
Output_1_105	G2 - 20	212.3	3.7	4.858	0.077
Output_1_106	G2 - 21	198.3	3.4	4.477	0.065
Output_1_107	G2 - 22	131.2	2	3.296	0.04
Output_1_108	G2 - 23	150.1	1.9	3.743	0.045
Output_1_109	G2 - 24	120.5	1.3	3.23	0.032
Output_1_110	G2 - 25	102.8	1.8	2.836	0.038

Output_1_111	G2 - 26	86.1	1.5	2.497	0.036
Output_1_112	G2 - 27	71.3	1.4	2.127	0.033
Output_1_113	G2 - 28	101.6	1.1	2.776	0.031
Output_1_114	G2 - 29	69.91	0.64	2.095	0.022
Output_1_115	G2 - 30	246.3	6.9	5.54	0.15
Output_1_116	G2 - 31	303.7	6.1	6.87	0.14
Output_1_117	G2 - 32	249.1	4.5	5.442	0.099
Output_1_118	G2 - 33	387.1	7.5	8.83	0.16
Output_1_119	G2 - 34	140.4	1.9	3.589	0.051
Output_1_120	G2 - 35	186.5	4	4.468	0.089
Output_1_121	G2 - 36	107.7	1.9	3.027	0.057
Output_1_122	G2 - 37	129.1	3.5	3.373	0.062
Output_1_123	G2 - 38	152.8	2.1	3.827	0.047
Output_1_124	Mica Mg - 31	158.6	1.7	1.872	0.018
Output_1_125	Mica Mg - 32	157.2	1.6	1.843	0.016
Output_1_126	Mica Mg - 33	157.5	1.4	1.856	0.014
Output_1_127	NIST 610 - 21	2.0482	0.0073	0.7087	0.0018
Output_1_128	NIST 610 - 22	2.0451	0.0081	0.7099	0.0014
Output_1_129	MDC - 31	41.52	0.39	1.0262	0.0072
Output_1_130	MDC - 32	41.99	0.49	1.0346	0.0091
Output_1_131	MDC - 33	42.02	0.34	1.0304	0.0084
Output_1_132	BCR - 21	0.3527	0.0038	0.7053	0.0028
Output_1_133	BCR - 22	0.3587	0.0035	0.7064	0.0031
Output_1_134	BR - 39	64.1	1.6	1.985	0.03
Output_1_135	BR - 40	95.03	0.94	2.6	0.027
Output_1_136	CR - 1	363.9	6.3	8.27	0.16
Output_1_137	CR - 2	370.5	5.8	8.54	0.17
Output_1_138	CR - 3	353.9	5.1	8.14	0.13
Output_1_139	CR - 4	76.8	1.2	2.347	0.025
Output_1_140	CR - 5	383.7	6.7	8.68	0.19
Output_1_141	CR - 6	444	10	9.44	0.22
Output_1_142	CR - 7	395.6	6.2	8.64	0.14
Output_1_143	CR - 8	430.4	9.5	9.12	0.21
Output_1_144	CR - 9	266.8	4.7	6.16	0.1
Output_1_145	CR - 10	277.4	6.2	6.39	0.14
Output_1_146	CR - 11	387.5	6.4	8.2	0.14
Output_1_147	CR Pro3 - 1	425	10	8.96	0.24
Output_1_148	CR Pro3 - 2	396.3	9.8	8.44	0.2
Output_1_149	CR Pro3 - 3	88.4	1.8	2.479	0.052
Output_1_150	CR - 12	374.8	8.3	8.1	0.17
Output_1_151	CR - 13	403.7	8.3	8.54	0.18
Output_1_152	CR - 14	461.1	9.4	10.27	0.22

Output_1_153	CR - 15	485	11	10.59	0.25
Output_1_154	Mica Mg - 34	154.3	1.5	1.837	0.016
Output_1_155	Mica Mg - 35	154.1	1.4	1.848	0.015
Output_1_156	Mica Mg - 36	153.4	1.4	1.851	0.015
Output_1_157	NIST 610 - 23	2.0426	0.0066	0.7097	0.0017
Output_1_158	NIST 610 - 24	2.0381	0.0073	0.7111	0.0015
Output_1_159	MDC - 34	41.63	0.43	1.0314	0.0076
Output_1_160	MDC - 35	41.59	0.41	1.0285	0.0083
Output_1_161	MDC - 36	41.72	0.35	1.041	0.0076
Output_1_162	BCR - 23	0.3507	0.0035	0.7065	0.003
Output_1_163	BCR - 24	0.3503	0.0037	0.7058	0.0026
Output_1_164	CR - 16	462	10	9.89	0.23
Output_1_165	CR - 17	451.2	9.1	10.2	0.23
Output_1_166	CR - 18	318.7	6.4	7.05	0.13
Output_1_167	CR Pro4 - 1	570	15	12.65	0.34
Output_1_168	CR - 19	423	12	9.06	0.24
Output_1_169	CR - 20	353.3	6.5	7.82	0.15
Output_1_170	CR - 21	441	11	9.77	0.24
Output_1_171	CR - 22	486	15	10.33	0.34
Output_1_172	CR - 24	290.6	8.8	6.51	0.23
Output_1_173	CR - 25	319.1	6.8	7.1	0.18
Output_1_174	CR - 26	318.4	8.3	6.75	0.19
Output_1_175	CR - 27	293	4.9	6.52	0.13
Output_1_176	CR - 28	283	6.2	6.11	0.14
Output_1_177	CR - 29	345.4	7.5	7.76	0.17
Output_1_178	CR - 30	310.6	6.3	6.99	0.13
Output_1_179	CR - 31	260.8	5.8	6.06	0.13
Output_1_180	CR - 32	337.2	5.2	7.87	0.12
Output_1_181	CR - 33	349.5	6.1	7.94	0.15
Output_1_182	CR - 34	340.7	5.5	7.76	0.13
Output_1_183	Mica Mg - 37	155.2	1.7	1.875	0.017
Output_1_184	Mica Mg - 38	149.1	1.1	1.852	0.016
Output_1_185	Mica Mg - 39	154	1.5	1.872	0.015
Output_1_186	NIST 610 - 25	2.0449	0.0071	0.7097	0.0017
Output_1_187	NIST 610 - 26	2.0385	0.0069	0.7094	0.0017
Output_1_188	MDC - 37	41.93	0.38	1.0376	0.0086
Output_1_189	MDC - 38	42	0.37	1.0362	0.0088
Output_1_190	MDC - 39	41.32	0.46	1.0302	0.0072
Output_1_191	BCR - 25	0.3536	0.0035	0.7058	0.0028
Output_1_192	BCR - 26	0.3529	0.0037	0.7054	0.003
Output_1_193	CR - 35	307.1	5.3	7.12	0.14
Output_1_194	CR - 36	310.9	5.4	7.24	0.14

Output_1_195	CR Pro1 - 1	378.1	7.9	8.16	0.19
Output_1_196	CR Pro1 - 2	347.7	7.8	7.62	0.2
Output_1_197	CR Pro1 - 3	333.9	7.3	7.4	0.18
Output_1_198	CR Pro2 - 1	282.3	8.7	6.98	0.21
Output_1_199	CR Pro2 - 2	344.1	6	7.9	0.16
Output_1_200	CR Pro2 - 3	337.8	7.1	7.65	0.17
Output_1_201	CR - 37	398.6	8.4	8.55	0.2
Output_1_202	CR - 38	285.1	5.6	6.47	0.14
Output_1_203	CR - 39	412.1	9.2	8.89	0.21
Output_1_204	CR - 40	399.5	9.6	8.67	0.22
Output_1_205	CR - 41	395.8	8.1	8.61	0.19
Output_1_206	CR - 43	343.5	5.3	7.96	0.15
Output_1_207	CR - 44	278.9	5.7	6.12	0.14
Output_1_208	CR - 45	245.8	4.7	5.589	0.099
Output_1_209	CR - 46	316.1	5.4	7.11	0.16
Output_1_210	G6 - 1	426	14	8.72	0.3
Output_1_211	G6 - 2	1107	55	22.6	1.1
Output_1_212	Mica Mg - 40	153.2	1.2	1.844	0.015
Output_1_213	Mica Mg - 41	152.9	1.2	1.852	0.016
Output_1_214	Mica Mg - 42	155.2	1.6	1.848	0.017
Output_1_215	NIST 610 - 27	2.0418	0.0078	0.7085	0.0018
Output_1_216	NIST 610 - 28	2.0432	0.008	0.7105	0.0018
Output_1_217	MDC - 40	41.75	0.42	1.0392	0.008
Output_1_218	MDC - 41	42.06	0.4	1.0303	0.0086
Output_1_219	MDC - 42	41.78	0.4	1.036	0.0068
Output_1_220	BCR - 27	0.3545	0.0034	0.7025	0.003
Output_1_221	BCR - 28	0.3543	0.0033	0.7022	0.0036
Output_1_222	G6 - 3	1050	67	23.1	1.4
Output_1_223	G6 - 4	433	17	9.39	0.37
Output_1_224	G6 - 5	553	20	10.94	0.37
Output_1_225	G6 - 7	948	64	18.4	1.2
Output_1_226	G6 - 8	324	12	7.18	0.26
Output_1_227	G6 - 9	905	41	18.77	0.88
Output_1_228	G6 - 10	300.5	8.5	6.81	0.23
Output_1_229	G6 - 11	15.68	0.64	1.006	0.032
Output_1_230	G6 - 14	209.2	7.9	4.79	0.2
Output_1_231	G6 - 15	817	31	16.42	0.6
Output_1_232	G6 - 16	883	57	18.8	1.3
Output_1_233	G6 - 21	291	19	6.92	0.42
Output_1_234	G6 - 22	411	18	8.63	0.39
Output_1_235	Mica Mg - 43	154.8	1.4	1.844	0.017
Output_1_236	Mica Mg - 44	154.7	1.6	1.865	0.017

Output_1_237	Mica Mg - 45	154.4	1.4	1.846	0.017
Output_1_238	NIST 610 - 29	2.0378	0.0073	0.7094	0.0015
Output_1_239	NIST 610 - 30	2.0342	0.0062	0.7091	0.002
Output_1_240	MDC - 43	41.2	0.4	1.026	0.0063
Output_1_241	MDC - 44	41.65	0.42	1.0416	0.0069
Output_1_242	MDC - 45	41.06	0.44	1.0347	0.0083
Output_1_243	BCR - 29	0.3582	0.0032	0.7055	0.0029
Output_1_244	BCR - 30	0.3579	0.0036	0.705	0.003
Output_1_245	G6 - 23	978	65	20.3	1.3
Output_1_246	G6 - 24	1163	70	24.3	1.4
Output_1_247	G6 - 25	526	36	11	0.76
Output_1_248	G6 - 26	586	28	12.37	0.65
Output_1_249	G6 - 27	836	36	17.24	0.76
Output_1_250	G6 - 28	610	27	11.66	0.5
Output_1_251	G6 - 29	285.5	8.9	6.03	0.2
Output_1_252	G6 - 30	812	51	17.5	1.2
Output_1_253	G6 - 31	454	16	9.05	0.35
Output_1_254	G6 - 32	2.18	0.1	0.743	0.016
Output_1_255	MDC test - 1	42.54	0.58	1.0299	0.0086
Output_1_256	MDC test - 2	41.83	0.39	1.0319	0.0082
Output_1_257	MDC test - 3	42.03	0.32	1.0372	0.007
Output_1_258	MDC test - 4	41.3	0.53	1.044	0.0067
Output_1_259	MDC test - 5	41.12	0.45	1.0366	0.0084
Output_1_260	MDC test - 6	40.39	0.55	1.0416	0.0076
Output_1_261	MDC test - 7	40.33	0.5	1.038	0.0079
Output_1_262	MDC test - 8	40.88	0.47	1.0358	0.0069
Output_1_263	MDC test - 9	40.69	0.46	1.0333	0.0076
Output_1_264	MDC test - 10	40.02	0.48	1.0285	0.0082
Output_1_265	Mica Mg - 46	151	1.4	1.846	0.015
Output_1_266	Mica Mg - 47	151.5	1.6	1.851	0.013
Output_1_267	Mica Mg - 48	148.4	1.4	1.858	0.015
Output_1_268	NIST 610 - 31	2.0323	0.0079	0.7106	0.0017
Output_1_269	NIST 610 - 32	2.0374	0.007	0.7106	0.0017
Output_1_270	MDC - 46	41.47	0.52	1.0353	0.0073
Output_1_271	MDC - 47	41.87	0.55	1.0427	0.0063
Output_1_272	MDC - 48	41.46	0.5	1.0376	0.0069
Output_1_273	BCR - 31	0.358	0.004	0.7026	0.0031
Output_1_274	BCR - 32	0.3552	0.0037	0.7083	0.0035
Output_1_275	G2 Pro - 1	161.8	2.5	4.17	0.066
Output_1_276	G2 Pro - 2	144.9	2	3.896	0.066
Output_1_277	G2 Pro - 3	148	1.7	3.912	0.062
Output_1_278	G2 Pro - 4	147.7	2.6	3.924	0.075

Output_1_279	G2 Pro - 5	159.7	3.3	4.143	0.089
Output_1_280	G2 Pro - 6	143.5	2.6	3.761	0.073
Output_1_281	G2 Pro - 7	132.6	2	3.559	0.049
Output_1_282	G2 Pro2 - 1	84.1	1.6	2.467	0.035
Output_1_283	G2 Pro2 - 2	458	9.2	9.98	0.21
Output_1_284	G2 Pro2 - 3	187	2.4	4.507	0.056
Output_1_285	G2 Pro2 - 4	197.1	3	4.704	0.074
Output_1_286	G2 Pro2 - 5	367	6.6	8.21	0.15
Output_1_287	G2 Pro2 - 6	383	7.1	8.59	0.18
Output_1_288	G2 Pro3 - 1	95.1	1.4	2.652	0.035
Output_1_289	G2 Pro3 - 2	84.97	0.98	2.423	0.027
Output_1_290	G2 Pro3 - 3	92.25	0.95	2.585	0.03
Output_1_291	G2 Pro3 - 4	98.2	1.3	2.737	0.04
Output_1_292	G2 Pro3 - 5	125.1	2.8	3.318	0.074
Output_1_293	CR Pro1 - 4	342.9	6.6	7.91	0.17
Output_1_294	CR Pro2 - 4	323.7	5.5	7.31	0.14
Output_1_295	CR Pro3 - 4	440.3	9.5	9.35	0.2
Output_1_296	CR Pro3 - 5	446.5	9	9.72	0.18
Output_1_297	CR Pro4 - 2	542	14	11.91	0.33
Output_1_298	CR Pro4 - 3	574	11	12.66	0.26
Output_1_299	CR Pro4 - 4	636	13	13.99	0.33
Output_1_300	Mica Mg - 49	155.9	1.8	1.849	0.015
Output_1_301	Mica Mg - 50	154.8	1.4	1.856	0.016
Output_1_302	Mica Mg - 51	156.1	1.6	1.855	0.014
Output_1_303	NIST 610 - 33	2.0414	0.0062	0.7087	0.0018
Output_1_304	NIST 610 - 34	2.0323	0.0069	0.7103	0.0018
Output_1_305	MDC - 49	40.28	0.32	1.0248	0.0079
Output_1_306	MDC - 50	41.1	0.33	1.0345	0.0086
Output_1_307	MDC - 51	41.47	0.39	1.0339	0.0093
Output_1_308	BCR - 33	0.3646	0.0033	0.7049	0.0033
Output_1_309	BCR - 34	0.3637	0.0032	0.7062	0.0028
		0.00100	0.00001	0.72607	0.00363

	Source file	StdCorr_Rb87	StdCorr_Rb87	StdCorr_Sr87	StdCorr_Sr87s_Sr86s_Int2SE
Output_1_1	Mica Mg - 1	161.7	1.5	1.842	0.018
Output_1_2	Mica Mg - 2	164.2	1.4	1.86	0.016
Output_1_3	Mica Mg - 3	164.5	1.2	1.864	0.017
Output_1_4	MDC - 1	40.46	0.37	1.0363	0.0058
Output_1_5	MDC - 2	40.19	0.37	1.0387	0.0066
Output_1_6	MDC - 3	39.89	0.36	1.0324	0.0062
Output_1_7	NIST 610 - 1	1.9938	0.0074	0.7095	0.0018
Output_1_8	NIST 610 - 2	1.9742	0.0063	0.7101	0.0015
Output_1_9	BCR - 1	0.3576	0.0037	0.71	0.0018
Output_1_10	BCR - 2	0.3576	0.0024	0.7026	0.002
Output_1_21	G1-1 - 1	2.551	0.053	0.822	0.019
Output_1_22	G1-1 - 2	2.784	0.043	0.827	0.012
Output_1_23	G1-1 - 3	2.749	0.061	0.837	0.02
Output_1_24	G1-1 - 4	2.848	0.037	0.849	0.012
Output_1_25	G1-1 - 5	2.563	0.038	0.835	0.012
Output_1_26	G1-1 - 6	2.98	0.043	0.841	0.011
Output_1_27	G1-1 - 7	2.871	0.036	0.844	0.011
Output_1_28	Mica Mg - 4	159.1	1.4	1.847	0.016
Output_1_29	Mica Mg - 5	158.7	1.2	1.856	0.015
Output_1_30	Mica Mg - 6	155.8	1.4	1.851	0.014
Output_1_31	MDC - 4	45.34	0.28	1.0659	0.0072
Output_1_32	MDC - 5	44.46	0.25	1.0593	0.0072
Output_1_33	MDC - 6	45.28	0.36	1.0648	0.0076
Output_1_34	NIST 610 - 3	2.03	0.0062	0.7109	0.0018
Output_1_35	NIST 610 - 4	2.0229	0.0057	0.7065	0.0014
Output_1_36	BCR - 3	0.3723	0.0024	0.7006	0.0023
Output_1_37	BCR - 4	0.3674	0.0021	0.7021	0.0024
Output_1_38	G1-1 - 8	2.369	0.041	0.805	0.014
Output_1_39	G1-1 - 9	2.222	0.034	0.82	0.013
Output_1_40	G1-1 - 10	2.715	0.033	0.817	0.011
Output_1_41	G1-1 - 11	2.585	0.034	0.837	0.012
Output_1_42	G1-1 - 12	2.918	0.05	0.837	0.016
Output_1_43	G1-1 - 14	0.02271	0.00092	0.7126	0.0042
Output_1_44	G1-1 - 15	2.46	0.038	0.818	0.011
Output_1_45	G1-1 - 16	2.176	0.042	0.819	0.015
Output_1_46	G1-1 - 17	2.789	0.04	0.822	0.013
Output_1_47	G1-1 - 18	0.2411	0.0073	0.7139	0.0048
Output_1_48	G1-2 - 1	38	2.2	2.44	0.1
Output_1_49	G1-2 - 2	37.27	0.86	1.929	0.028
Output_1_50	G1-2 - 3	58.8	2.4	3.04	0.18
Output_1_51	G1-2 - 4	0.3009	0.0038	0.7337	0.0039
Output_1_52	G1-2 - 5	2.058	0.05	0.811	0.017
Output_1_53	G1-2 - 7	0.2556	0.008	0.7344	0.0061
Output_1_54	G1-2 - 8	0.8664	0.0081	0.7539	0.0052
Output_1_55	G1-2 - 9	0.751	0.014	0.7517	0.0026
Output_1_56	Mica Mg - 7	165.8	1.5	1.828	0.016
Output_1_57	Mica Mg - 8	165.2	1.3	1.871	0.013
Output_1_58	Mica Mg - 9	164.7	1.4	1.863	0.015
Output_1_59	MDC - 7	40.8	0.3	1.0387	0.007
Output_1_60	MDC - 8	40.62	0.25	1.0201	0.0072
Output_1_61	MDC - 9	40.65	0.25	1.0151	0.0072
Output_1_62	NIST 610 - 5	1.9942	0.0068	0.7112	0.0015
Output_1_63	NIST 610 - 6	2.0096	0.0067	0.7053	0.0014
Output_1_64	BCR - 5	0.3653	0.0031	0.71	0.0022
Output_1_65	BCR - 6	0.3552	0.0033	0.7115	0.002

Table 6: Raw data and profiles for all the samples used for LA-QQQ. Using Mica Mg, NIST 610, MDC and BCR as standards. Note that, CR is another mount of the sample G2. "G1" on the last represents G10.